



1352-2310(94)00319-X

A MODEL INVESTIGATION OF SUMMERTIME DIURNAL OZONE BEHAVIOR IN RURAL MOUNTAINOUS LOCATIONS

RAHUL A. ZAVERI,* RICK D. SAYLOR,† LEONARD K. PETERS,*
RICHARD McNIDER‡ and AARON SONG‡

*Department of Chemical Engineering, Virginia Polytechnic Institute and State University, Blacksburg, VA 24061, U.S.A.; †Earth and Environmental Sciences Center, Pacific Northwest Laboratory, Richland, WA 99352, U.S.A. and ‡Earth System Sciences Laboratory, University of Alabama in Huntsville, Huntsville, AL 35899, U.S.A.

(First received 27 May 1994 and in final form 25 September 1994)

Abstract—The STEM-II pollutant transport, transformation, and deposition model has been used to simulate diurnal patterns of surface ozone concentration at idealized high-elevation mountaintop locations and low-elevation plains and valley sites. Two-dimensional hydrostatic mesoscale simulations, initialized with atmospheric conditions representative of sunrise over the southern Appalachians on 19 June, were used to generate meteorological data to drive STEM-II simulations. Sensitivity of surface ozone concentrations has been investigated against input initial and background vertical profiles, synoptic wind speed, photochemistry, and surface removal. The model reproduced typical surface ozone concentration diurnal patterns observed at several high- and low-elevation sites in the United States and central Europe. Results indicate that the nighttime high ozone concentrations at high-elevation mountainous locations are primarily due to the occurrence of local topographically induced wind systems which transport ozone-rich air from aloft down mountain slopes. The simulations indicate that in some situations higher ozone concentrations may also be observed at mountaintop locations due to transport of residual ozone-rich air masses above the nocturnal boundary layer to high-elevation locations.

Key word index: Photochemistry, ozone exposure, high-elevation, numerical simulations.

1. INTRODUCTION

During the past two decades, a marked forest decline has been observed in the high-elevation environment of the Appalachian mountains in the eastern United States, and in central Europe (Lefohn and Runeckles, 1987; Woodman and Cowling, 1987; Lovett and Kinsman, 1990; Proyou *et al.*, 1991; Aneja and Li, 1992). Ozone, the most prevalent photochemical oxidant in the atmosphere, in sufficiently high concentration (50 ppbv or more), is believed to influence forest health adversely (Reich and Amundson, 1985).

Several field studies (e.g. Fehsenfeld *et al.*, 1983; Galbally *et al.*, 1986; Angle and Sandhu, 1989; Peake and Fong, 1990; Wunderli and Gehrig, 1990; Aneja *et al.*, 1991; Aneja and Li, 1992) have indicated that the diurnal behavior of surface ozone concentrations is distinctly different at high-altitude mountainous sites as compared to lower-elevation valley and plain locations. Typically, low-elevation areas exhibit a mid-afternoon maximum corresponding to the period of greatest vertical mixing and photochemical activity, and a nighttime minimum when there is

a lack of photochemical ozone production and continued removal via surface deposition coincident with possible NO scavenging. The above-mentioned studies have reported that high-elevation mountainous sites continuously experience significantly higher ozone exposure with little or no diurnal variation, and in some cases exhibit a weak reversed diurnal signal with a nighttime maximum. While elevational gradients in ozone concentration in the troposphere may partly explain the overall higher ozone exposure at high-elevation mountainous locations (Warneck, 1988; Aneja *et al.*, 1991), the causes for weak or reversed diurnal ozone signals observed at these sites are still not clear. The combination of several physical and chemical processes coupled with topographically induced wind systems are suspected to be involved in the phenomenon (Aneja *et al.*, 1991).

Several mechanisms have been proposed to explain the different diurnal behaviors of rural ozone concentrations at low-elevation plains and valleys and high-elevation mountainous locations. At low-elevation sites, physical and chemical atmospheric processes, coupled with the diurnal evolution of the

atmospheric boundary layer, govern the near-surface behavior of ozone mixing ratios. Over homogeneous continental terrain under clear-sky conditions, the boundary layer has a well-defined structure that evolves with a diurnal cycle. The typical diurnal behavior of surface ozone mixing ratio at low-elevation locations is due primarily to turbulent downward mixing of ozone from above the nocturnal boundary layer as the convective mixed layer grows shortly after sunrise, with further increases due to photochemical production from ozone precursors which are possibly transported into the residual layer above rural areas during the previous night or early morning (Fehsenfeld *et al.*, 1983). The nighttime decrease in surface ozone concentration is mainly due to dry deposition at the ground (Harrison *et al.*, 1978; Fehsenfeld *et al.*, 1983; Kelly *et al.*, 1984; Fontan *et al.*,

1992). Helas *et al.* (1987) showed evidence of nocturnal scavenging of ozone by nitric oxide originating from soil; however, this effect remains confined very close to the ground in the absence of turbulence in an extremely stable nocturnal surface layer.

For there to be a different type of diurnal behavior at mountainous, high-elevation sites, some perturbation of the above mechanisms must occur. During the diurnal cycle in the mountainous regions, local wind circulations can form within and just above the valleys as illustrated schematically in Fig. 1. After sunset, radiative cooling of the mountain slopes cools the adjacent air, resulting in shallow cold downslope flows or *katabatic winds* on the order of 1 to 5 m s^{-1} (McNider and Pielke, 1984; Broder and Gygas, 1985; Stull, 1988). These winds may transport ozone-rich upper layer air to the mountaintop and slopes,

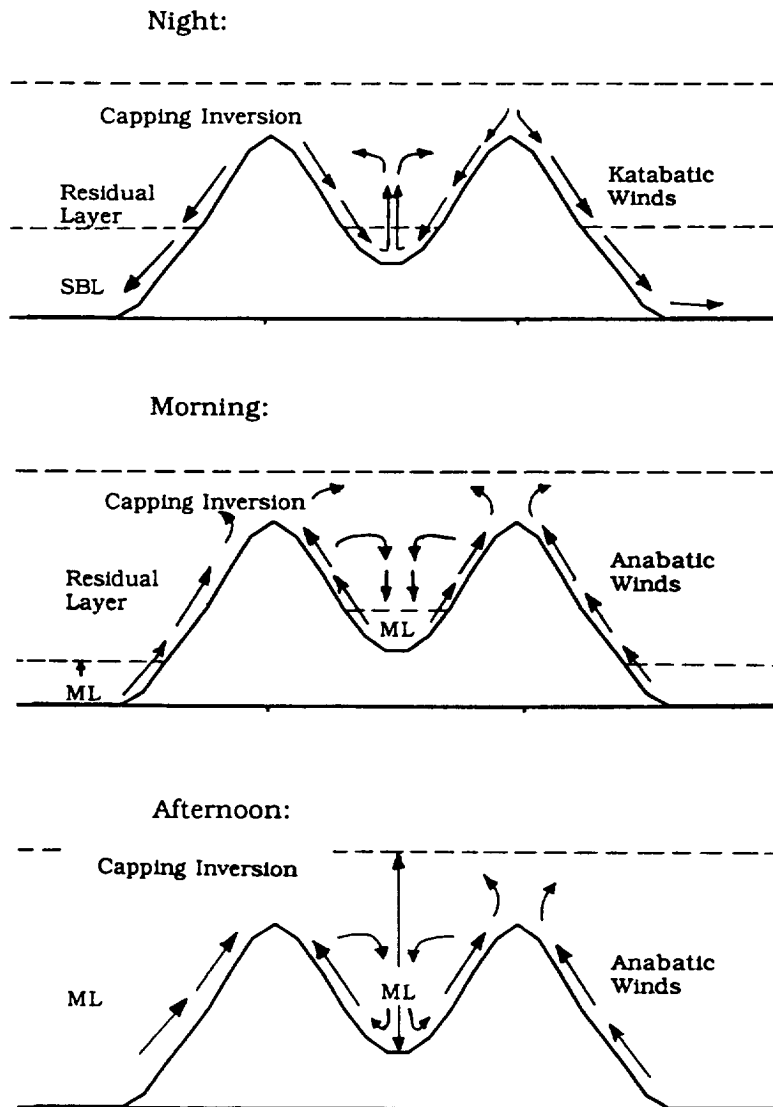


Fig. 1. Idealized BL evolution over mountainous terrain (adapted from Broder *et al.*, 1981, and Stull, 1988).

compensating, when the mountaintop is above the nocturnal boundary layer (NBL), for any depletion caused by dry deposition or nocturnal chemical scavenging. Another factor may be that the maintenance of shear aloft in the katabatic flows never allows the surface to be decoupled. The shear maintains a level of turbulent connectivity between the surface and the ozone-rich air aloft so that surface ozone levels remain high. Above the valley floor, there is a gentle upward airflow to maintain mass conservation. The katabatic winds continue throughout the night, resulting in a stably stratified pool of cold air in the valley, often called the *valley inversion*. Thus, the NBL or SBL (stable boundary layer) above the valley develops a lower ozone content at the surface due to continued destruction via surface deposition and nighttime atmospheric chemical reactions.

Shortly after sunrise, solar heating warms the air adjacent to the slopes, causing a reversal in the direction of the mountain-slope winds, giving rise to upslope or *anabatic winds*. Above the valley inversion, there is gentle convergence and subsidence. As the surface heating continues, the growing mixed layer (ML) eventually breaks the valley inversion, gradually eliminating concentration gradients in the vertical. These local wind system effects are most marked during periods of weak ambient winds. In many actual cases, however, mean synoptic winds tend to modify the circulation patterns and hence the pollutant concentrations at the surface.

This study is an investigation of some of the potential mechanisms that may produce the observed differences in diurnal ozone behavior between low- and high-elevation mountainous locations. Our investigation was accomplished via computer simulation of the atmospheric system using STEM-II (Carmichael *et al.*, 1991), an Eulerian photochemical oxidant numerical model. The STEM-II model was driven by realistic meteorological data and wind fields from simulations produced by the two-dimensional hydrostatic mesoscale model of McNider and Pielke (1984). Since coupled meteorological and chemical models of the type used here will probably be used for future environmental impact and regulatory studies, it is important that there be an understanding of whether such model systems can correctly reproduce this differential diurnal behavior.

2. THE MODELING SYSTEM

2.1. Meteorological model

The meteorological model is a hydrostatic, primitive-equation model, originally developed by Pielke (1974), Pielke and Mahrer (1975), Mahrer and Pielke (1977, 1978), and McNider and Pielke (1981). The basic governing equations are transformed from Cartesian coordinates to a terrain-following coordinate system. The temperature at the air-ground

interface is calculated using an energy budget where the shortwave and longwave radiation, the soil heat flux, and the turbulent mixing of sensible and latent heat are used to determine the equilibrium surface temperature. The surface layer fluxes of heat, moisture, and momentum are based on the work of Businger *et al.* (1971), while the turbulent mixing in the remainder of the planetary boundary layer (PBL) is parameterized using an exchange coefficient formulation described in O'Brien (1970). The depth of the PBL is predicted using the formulation of Deardorff (1974). Further details of the meteorological model will be presented in a future paper.

2.2. STEM-II photochemical model

The Sulfur Transport Eulerian Model, version 2 (STEM-II) has been tested extensively and applied to a number of regional, mesoscale, and urban acid deposition and photochemical oxidant simulations. These include a study of long-range transport and formation of photochemical oxidants in central Japan involving land/sea breeze and mountain/valley winds (Chang *et al.*, 1989), and more recently, a study of mesoscale acid deposition in the lower Ohio River Valley (Saylor *et al.*, 1991). The gas-phase chemistry module of STEM-II is based on the photochemical oxidant mechanism of Atkinson *et al.* (1982), which includes 86 chemical reactions of 55 species. Details of the STEM-II model formulation and numerics can be obtained in Carmichael *et al.* (1991).

In the present work, the STEM-II model has been used to simulate the chemistry and dry deposition processes coupled with topographically induced wind systems that govern the diurnal behavior of surface ozone concentrations in rural mountainous regions. An idealized two-hill topography was mapped into a two-dimensional (in the horizontal and vertical) domain oriented along 36°N latitude and extending from 85°W to 86.7°W longitude, and chosen to be representative of the southern Appalachian mountains (Fig. 2). The vertical extent of the 2-D domain is 5.3 km and is discretized in a non-uniform fashion, with mesh size becoming coarser with increasing altitude. The vertical levels in the lowest 500 m are centered at 5, 15, 30, 60, 100, 154, 210, 290, 382, and 499 m above the surface. The east-west horizontal extent of the domain is 152 km and is uniformly discretized with a 2 km grid node spacing. The idealized mountain peaks are located at horizontal grid nodes 50 and 61, have an altitude of 0.95 km, and an average slope gradient of 7.2%.

The meteorological data sets for clear-sky atmospheric conditions consisted of hourly fields of temperature, humidity, air density, wind velocity (horizontal and vertical components), and eddy diffusivity. These fields were generated separately in two-dimensional hydrostatic mesoscale simulations and then processed for use by the STEM-II model in offline chemical simulations. Three hydrostatic simulations were performed, each with a different

synoptic westerly wind speed (1, 3, and 5 m s⁻¹), and were initialized with atmospheric conditions representative of sunrise (0500 CDT) over the southern Appalachians on 19 June. Details of the meteorological data fields can be found in Zaveri (1993).

A diurnally varying dry deposition velocity for O₃ was specified using the observed diurnal curves for Julian days 189–243 at the Borden forest, a fully leafed, mixed deciduous forest located on the Canadian Forces Base Borden (Padro *et al.*, 1991).

The observed half-hourly averaged diurnal curve was visually smoothed, and hourly values were used for STEM-II simulations. Diurnal dry deposition curves for NO, NO₂, HNO₃, PAN, and NMHC were constructed by scaling the observed daytime average values (Hanson and Lindberg, 1991; Chang *et al.*, 1989) according to the diurnal behavior of O₃ dry deposition velocity (refer to Fig. 3). Deposition velocities were prescribed uniformly across the domain surface at plains, valley, and mountain grid nodes.

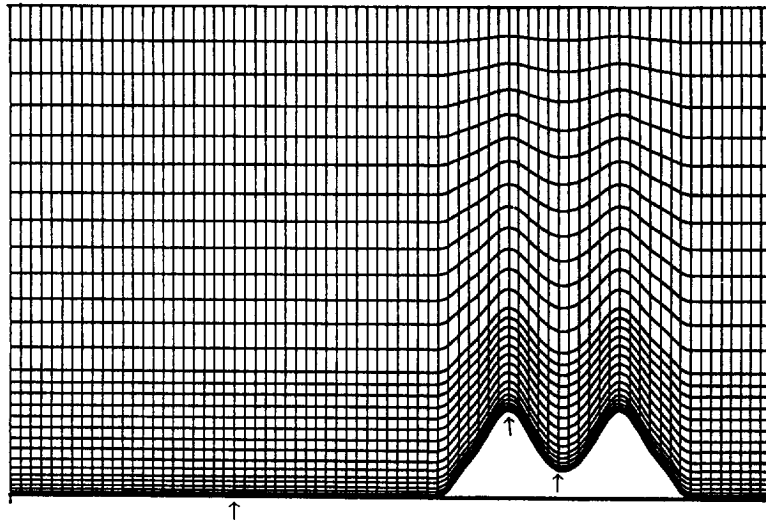


Fig. 2. Terrain-following grid system with idealized two-hill topography. Arrows indicate locations of nodes for Figs 5, 6, and 8.

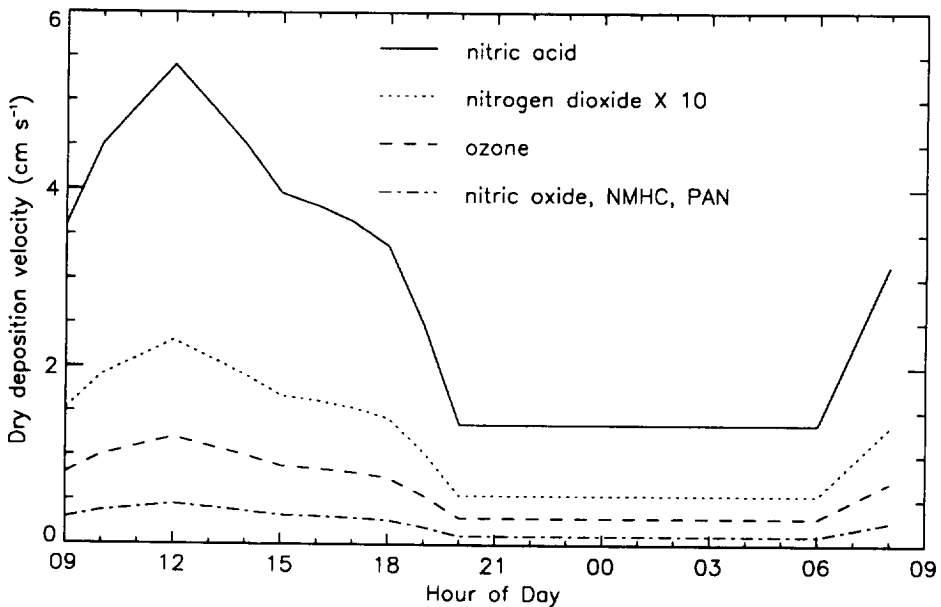


Fig. 3. Diurnal curves of dry deposition velocity for O₃, NO₂, NO, HNO₃, PAN, and NMHC.

Table 1. Organization of simulations

Initial and background conc. profiles	Synoptic wind speed (m s^{-1})	Chemistry	Dry deposition velocity	Number of simulations
(a)	1.0	On	Constant	12
	3.0	Off	Diurnally varying	
	5.0			
(b)	1.0	On	Constant	12
	3.0	Off	Diurnally varying	
	5.0			
(c)	1.0	On	Constant	12
	3.0	Off	Diurnally varying	
	5.0			
(d) Flat terrain	3.0	On	Diurnally varying	2
		Off		
Total				38

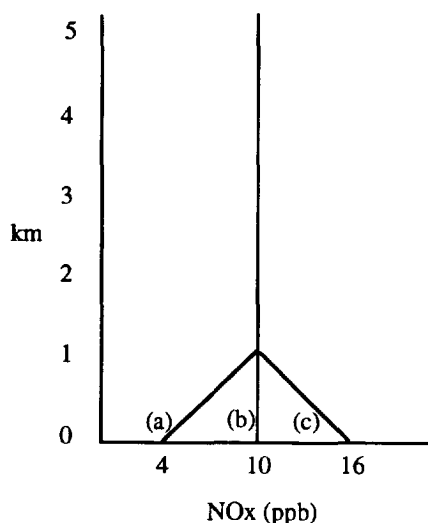
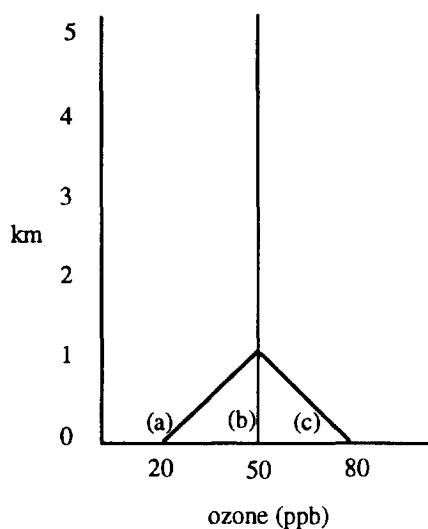


Fig. 4. Initial and background gas-phase vertical concentration profiles.

3. ORGANIZATION OF SIMULATIONS

Thirty-eight numerical experiments were performed to investigate the sensitivity of surface ozone concentrations to input initial and background vertical concentration profiles, synoptic wind speed, photochemistry, and diurnal variations in dry deposition velocities (Table 1). The variations in these parameters and the underlying rationale for their selection were as follows:

1. Three initial and background vertical profiles of input species, as shown in Fig. 4, represent three levels of pollutant concentrations in the boundary layer. With a synoptic westerly wind, the profiles (a), (b), and (c) represent an air mass advected into the domain from remote rural, suburban or rural, and urban or industrial areas, respectively. The effect of vertical mixing was also investigated by observing subsequent changes occurring in these vertical profiles with diurnally evolving boundary layer properties.

2. Synoptic westerly wind speeds of 1, 3, and 5 m s^{-1} represent the decreasing age of air masses reaching the rural mountainous area. Also, the strengths of the upslope/downslope flows are affected somewhat by the magnitude of the synoptic flow.

3. The effect of photochemistry was observed by simply turning the chemistry module on or off. Turning chemistry off also simplifies the analysis of dry deposition and vertical mixing effects.

4. The effect of surface removal was investigated by either allowing dry deposition velocities to vary diurnally or setting them to constant minimum values.

5. Lastly, the influence of horizontal advection was separated from the influences attributed to the topography of the model by performing two flat terrain simulations with uniform vertical profile (b), 3 m s^{-1} synoptic wind speed, diurnally varying dry deposition velocity, and chemistry turned on and off.

Background and initial distributions of a specified NO_x mixing ratio were split into NO and NO_2 according to the photostationary state relation between O_3 , NO_2 , and NO (without hydrocarbons). During nighttime, all background NO_x was assumed to be present solely as NO_2 . The total non-methane hydrocarbon (NMHC) background mixing ratio distribution was based on a ppb C : ppb NO_x ratio set equal to 5. The composition of the hydrocarbon distribution was imposed according to the median concentrations of the 25 most abundant compounds in 39 U.S. cities as given by Seinfeld (1989). The hydrocarbons were apportioned into surrogate categories according to the lumping scheme of Atkinson *et al.* (1982). Table 2 shows the composition of the NMHC mix as ppb C corresponding to a total NMHC concentration of 100 ppb C.

Table 2. Composition of hydrocarbon mix

NMHC species	Carbon mixing ratio (ppb C)
Alkane	60.4
Propane	7.00
Propene	2.30
Butene	1.76
Ethene	6.40
Benzene	3.75
Toluene	10.0
Xylene	5.40
Formaldehyde	0.83
Acetaldehyde	1.73
Higher aldehydes	0.43

In the following discussion, the simulations are identified according to the input meteorological and modeling conditions. As examples: simulation (b-1-off-c) denotes the case with profile (b), mean synoptic wind speed of 1 m s^{-1} , chemistry off, and constant dry deposition velocities; ensemble (avg-on-d) denotes an average of nine cases with chemistry on and diurnally varying dry deposition. The nine cases differ in mean wind speeds (1, 3, and 5 m s^{-1}) and background vertical profiles (a, b, and c).

4. RESULTS AND DISCUSSION

STEM-II simulation results consist of hourly mixing ratio fields of all computed species. All simulations were carried out for 48 h of model time; however, in order to minimize effects of initial species distributions, only the last 24 h were used for analysis. In the following, only ozone fields are presented and discussed; further simulation results, including profiles of NO_x , NO_y , PAN and other species, can be found in Zaveri (1993).

4.1. Diurnal patterns of surface ozone concentrations

Hourly simulated mixing ratios of ozone were plotted for several grid node locations to obtain simulated diurnal patterns that are comparable to actual measured diurnal averages at mountainous and low-elevation monitoring sites. The chosen grid nodes (see Fig. 2) are located over the western plain, mountaintop, and valley bottom at a height of 15 m above ground-level (model level 2). The western plains location was placed 46 km (horizontal grid node 23) from the modeling domain's western boundary to

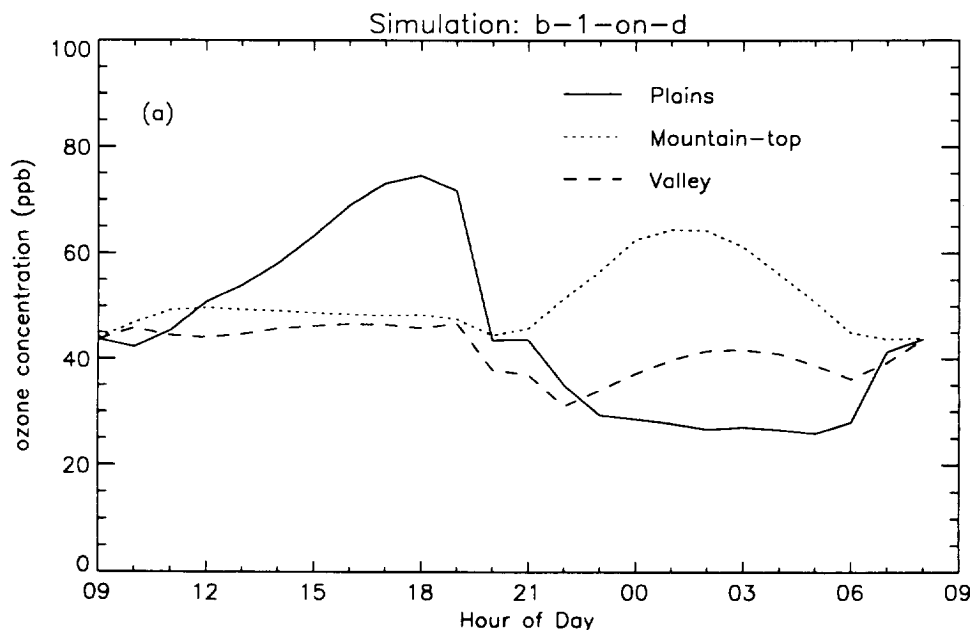


Fig. 5. (a).

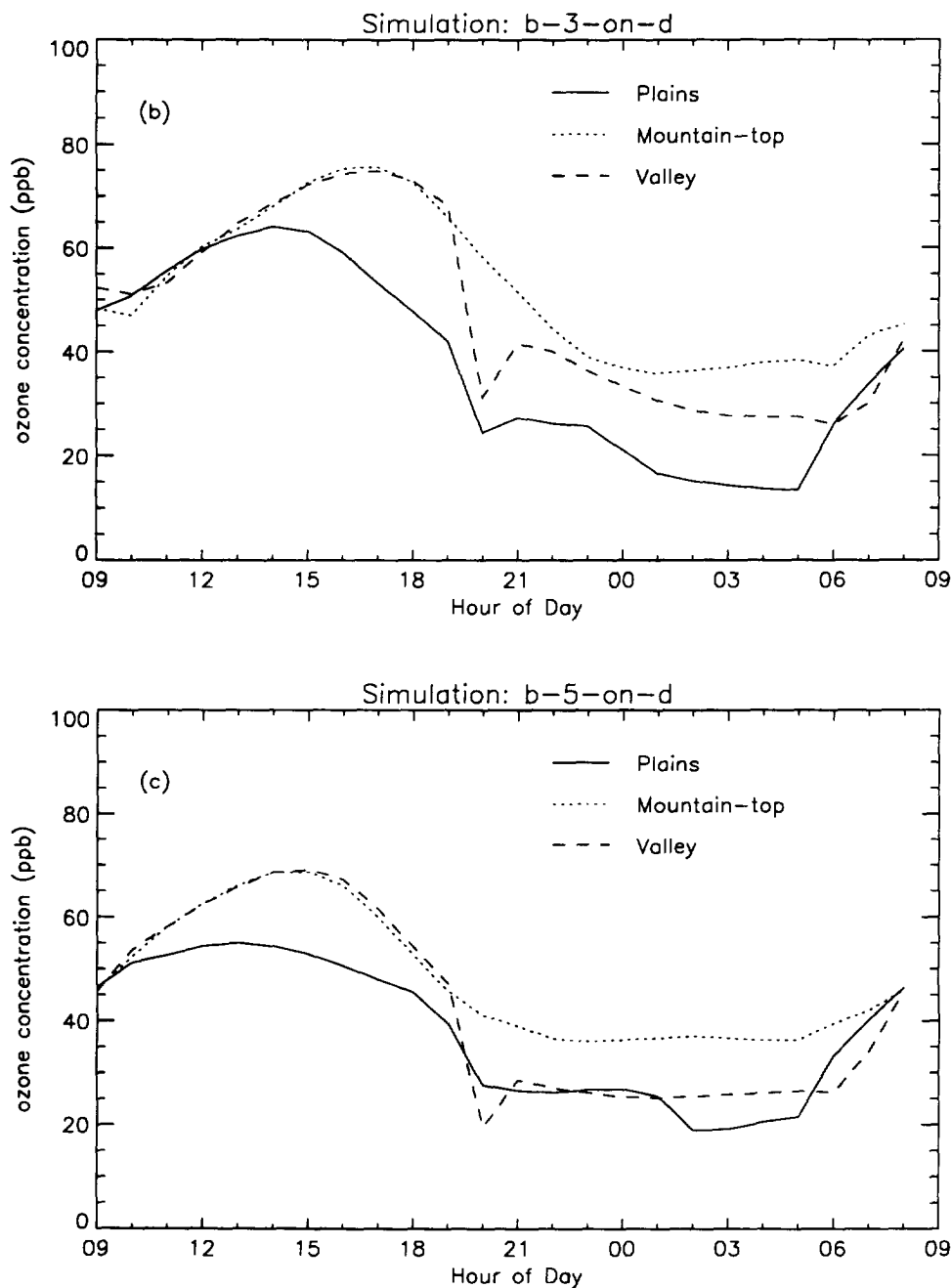


Fig. 5. Diurnal ozone concentration curves (ppb) over western plains, mountaintop, and valley for simulations: (a) b-1-on-d; (b) b-3-on-d; and (c) b-5-on-d.

minimize the influence of boundary conditions and to minimize the influence of drainage flows from the western mountain slope. The mountaintop and valley sampling points were at an altitude of 965 m (horizontal grid node 50) and 304 m (horizontal grid node 55) above mean sea-level, respectively.

Figures 5a-c show diurnal ozone plots for individual simulations with background profile (b), chemistry on, diurnally varying dry deposition velocities, and three synoptic wind speeds. All three

cases show a typical daytime increase in ozone over the plains due to photochemical production. A considerable difference is observed in the occurrence of ozone concentration peaks at the mountaintop with increasing synoptic wind speeds. For simulation (b-1-on-d) the mountaintop location experiences a maximum ozone mixing ratio between 0100 CDT and 0200 CDT, reflecting transport of ozone contained within the residual boundary layer from the previous day. In all cases of Fig. 5, the

mountaintop site experiences greater nighttime ozone mixing ratios than either the plains or valley locations. These figures illustrate the sensitivity of rural surface ozone concentrations to synoptic wind speed, and to *in situ* and in-transit photochemical production of ozone when ozone precursors are transported to rural areas.

Figures 6a–c are plots of simulated diurnal ozone behavior for simulations (a-3-off-c), (b-3-off-c), and (c-3-off-c). Since in these simulations chemistry is

turned off within the model, no significant increases in daytime ozone values occur. However, each of the different initial and background profiles produced the typical diurnal patterns at the plains, mountaintop, and valley. Also, even though the surface removal continues throughout the daytime, surface ozone values stay at relatively high values until just before sunset (2000 CDT). This is the result of intense boundary layer turbulence that mixes down ozone-rich air from aloft. When the boundary layer

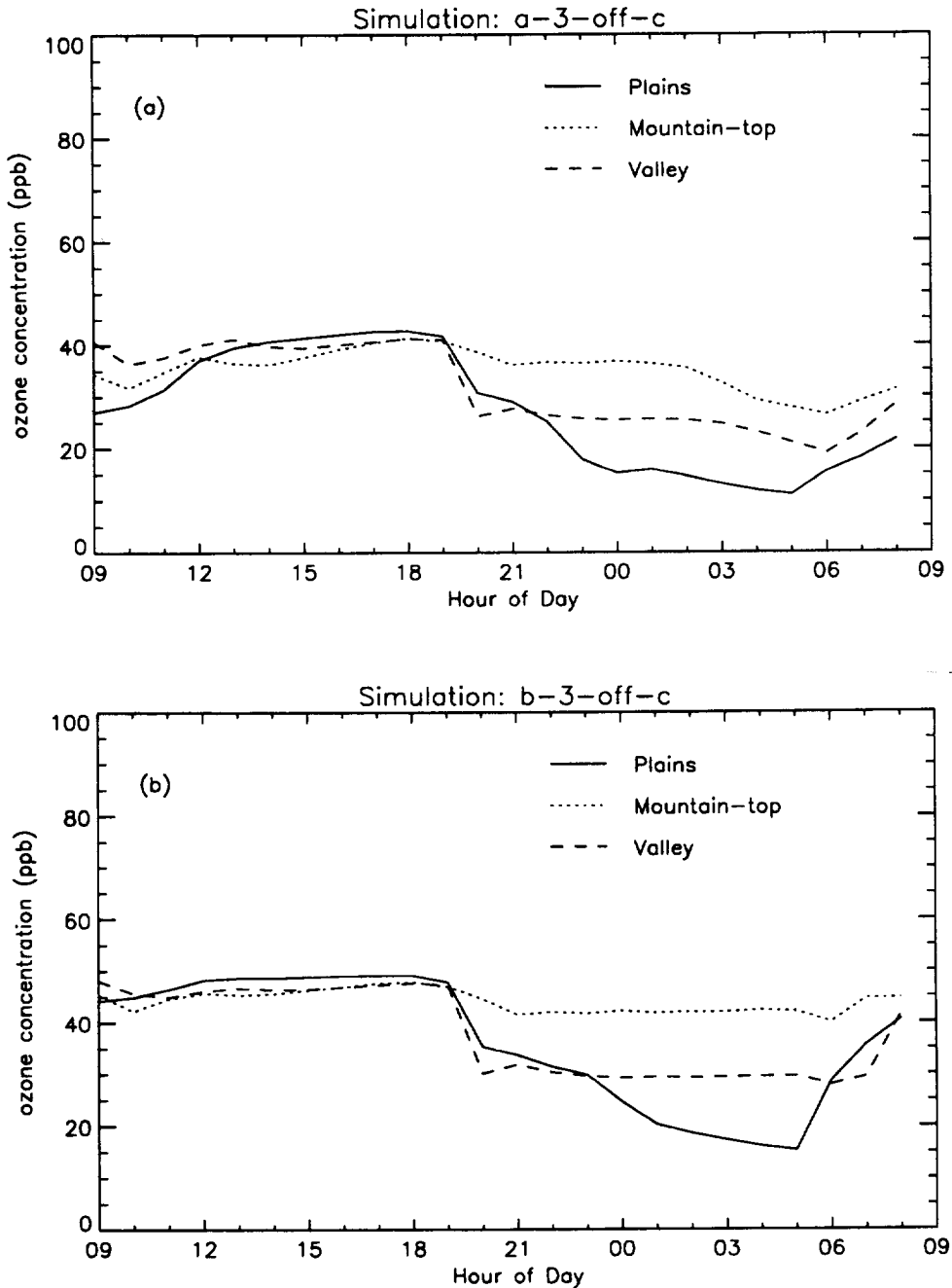


Fig. 6. (a, b).

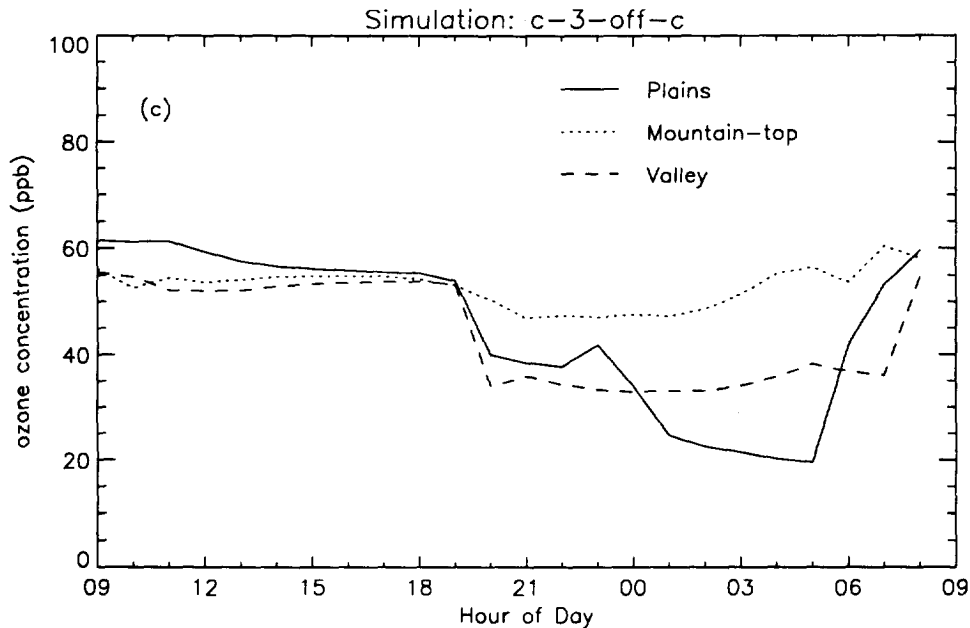


Fig. 6. Diurnal ozone concentration curves (ppb) over western plains, mountain-top, and valley for simulations: (a) a-3-off-c; (b) b-3-off-c; and (c) c-3-off-c.

begins to break down just before sunset, surface removal begins to have a discernible effect and ozone values near the surface begin falling. Nighttime surface removal continues until sunrise (0500 CDT) when new boundary layer mixing begins, again bringing down ozone from the previous day's residual layer.

As was seen in Fig. 5, nighttime mountaintop ozone levels remain higher than those at the plains and valley locations for the chemistry off simulations of Fig. 6. Nighttime surface removal does not deplete mountaintop ozone levels as much as at the other sites because a continuous supply of ozone-rich air is advected from aloft by the nighttime downslope flow. To a lesser extent, the valley location also is affected by ozone advected downslope, and, consequently, ozone levels there are not depleted as much as at the plains location.

The effects of horizontal advection and influences from the mountainous terrain induced flows can be clearly seen by comparing Fig. 5b with Fig. 7a. The diurnal patterns of ozone concentration produced at the plains location are similar for the simulations with mountainous or flat terrains. However, the western mountaintop and valley locations clearly show weaker diurnal variations as compared to the flat terrain results over corresponding locations, indicating the important role of nighttime terrain induced flows. Similar delays in ozone concentration peaks are seen in both simulations, indicating the effect of horizontal advection on in-transit photochemical production of ozone. The flat terrain simulation with chemistry off also illustrates the influence of terrain

induced flows in the mountainous terrain simulations, as well as clarifying the influence of daytime photochemistry on the diurnal pattern of ozone concentration at different locations (compare Figs 6b and 7b).

Figures 8a–d present simulated ensemble average ozone curves which show a weaker diurnal variation of ozone mixing ratio on the western mountaintop than that produced at the plains and valley locations. For comparison, a few selected observed diurnal ozone mixing ratio patterns at low and high elevations are shown in Figs 9a and b. The simulation results of Fig. 8 compare quite well with the observed diurnal patterns. Differences in the amplitude of the diurnal cycle between the simulated and observed data are likely due to differences in the levels of NO_x and hydrocarbons, as well as differences in the amount of ozone removed at the surface.

4.2. Vertical profiles of ozone concentrations

Vertical profiles of ozone concentrations at 3 h intervals for two base simulations (b-3-off-d and b-3-on-d) are shown in Figs 10a–h and 11a–h. In simulation (b-3-off-d) with chemistry inactive (Fig. 10), changes in ozone distribution are due only to transport, surface removal, and turbulent mixing. During daytime, ozone is removed at the surface, while vigorous mixing within the boundary layer redistributes the remaining ozone relatively uniformly. As surface removal of ozone begins to decrease in the late afternoon (see Fig. 3), advection of background ozone from the western boundary becomes more important. After sunset, when

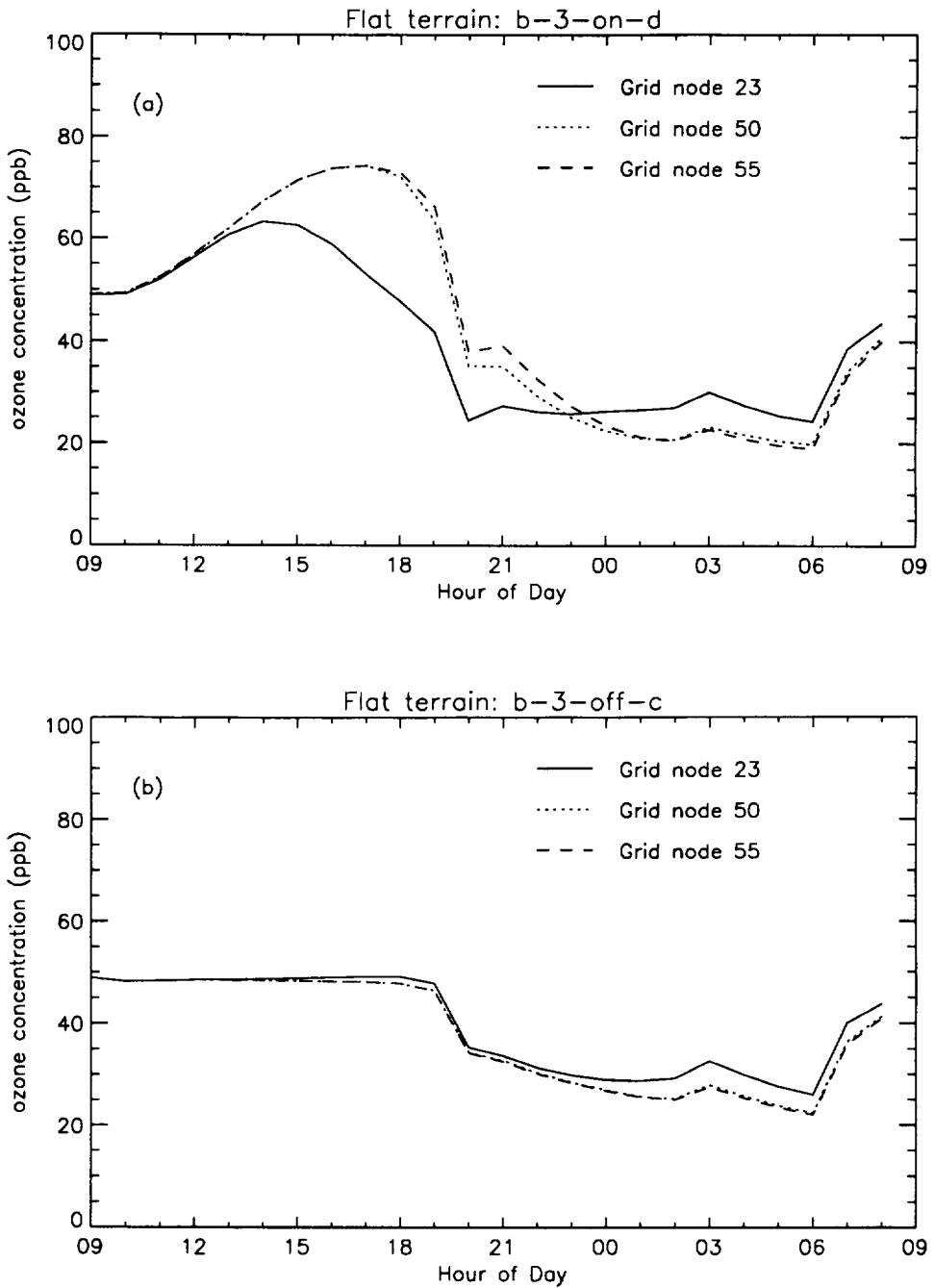


Fig. 7. Diurnal ozone concentration curves (ppb) over grid nodes 23, 50, and 55 for flat terrain simulations: (a) b-3-on-d; and (b) b-3-off-c.

turbulent mixing in the boundary layer has been greatly reduced, surface removal again becomes pronounced, leading to depletion of near-surface ozone in the plains and valley. However, depletion of ozone does not occur at the mountaintops due to downward advection of ozone-rich air from aloft. Ozone advection down the slopes of the mountains is observed at both 2100 CDT and 2400 CDT. In fact, a front of elevated ozone moves down the western side

of the western mountain and is lifted above the developing nocturnal boundary layer by 0300 CDT.

In simulation (b-3-on-d) where chemistry is active (Fig. 11), the transport dynamics are exactly the same; however, ongoing photochemical processes lead to higher ozone values and more complex mixing ratio distributions. During the morning hours, ozone is produced photochemically in an area above the mountaintops. Early in the afternoon (1500 CDT),

significant amounts of ozone have been produced throughout the domain, with peaks occurring to the west of and above the mountains. In the later afternoon (1800 CDT), as photochemical production of ozone begins to wane, westerly advection of the residual ozone above the mountains begins to become important. Some destruction of ozone aloft occurs, primarily due to titration with nitric oxide; however, this is short-lived since NO is rapidly depleted. After

sunset, as with simulation (b-3-off-d), surface removal of ozone becomes evident over the plains and in the valley, but not at the mountaintops. As before, downslope flows continuously transport ozone from aloft to the mountaintop and down its slopes, replenishing any losses due to surface removal. At 2100 CDT an air mass containing residual ozone from aloft flows down the western side of the western mountain. Throughout the nighttime, the downslope

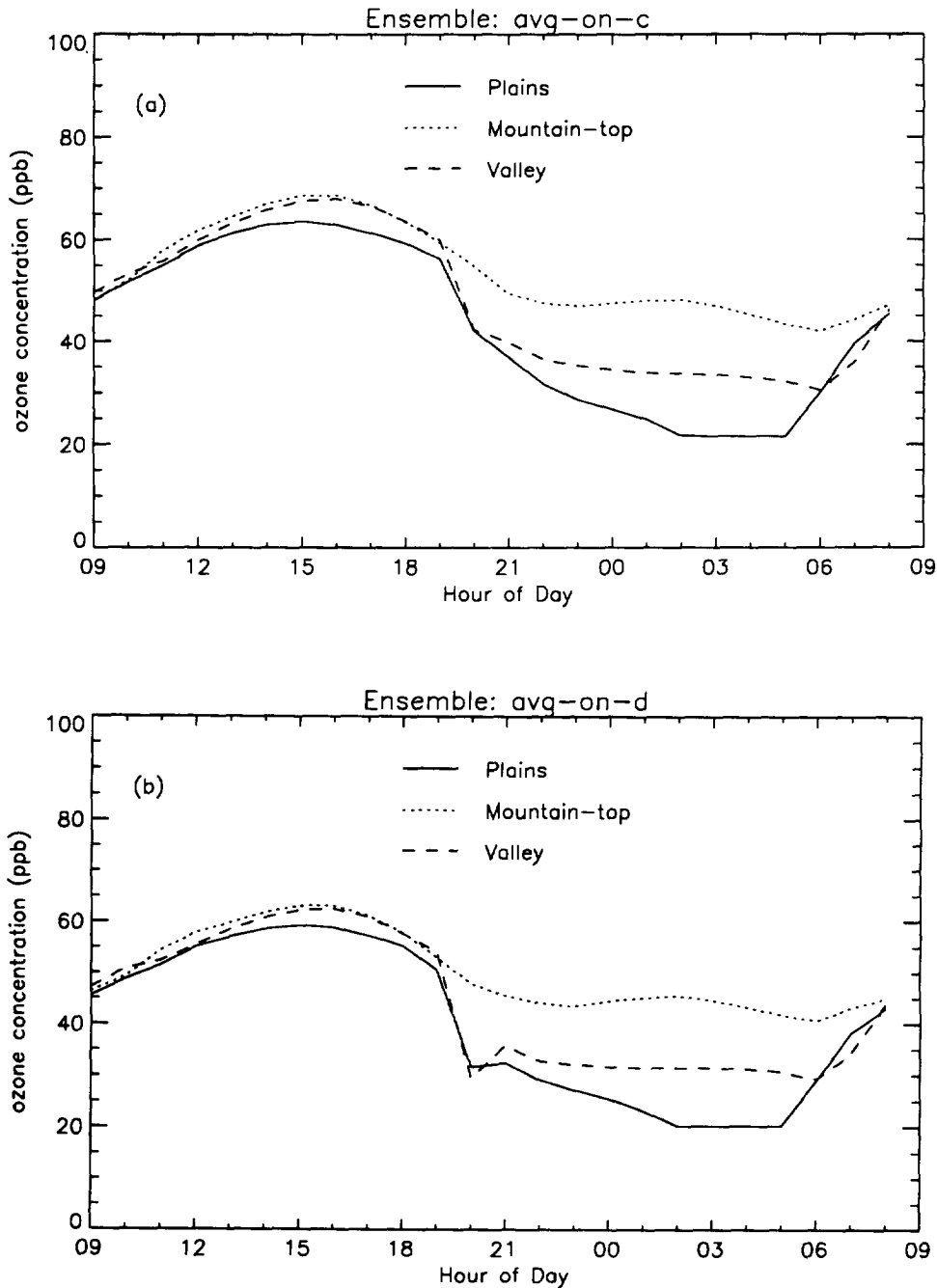


Fig. 8. (a, b).

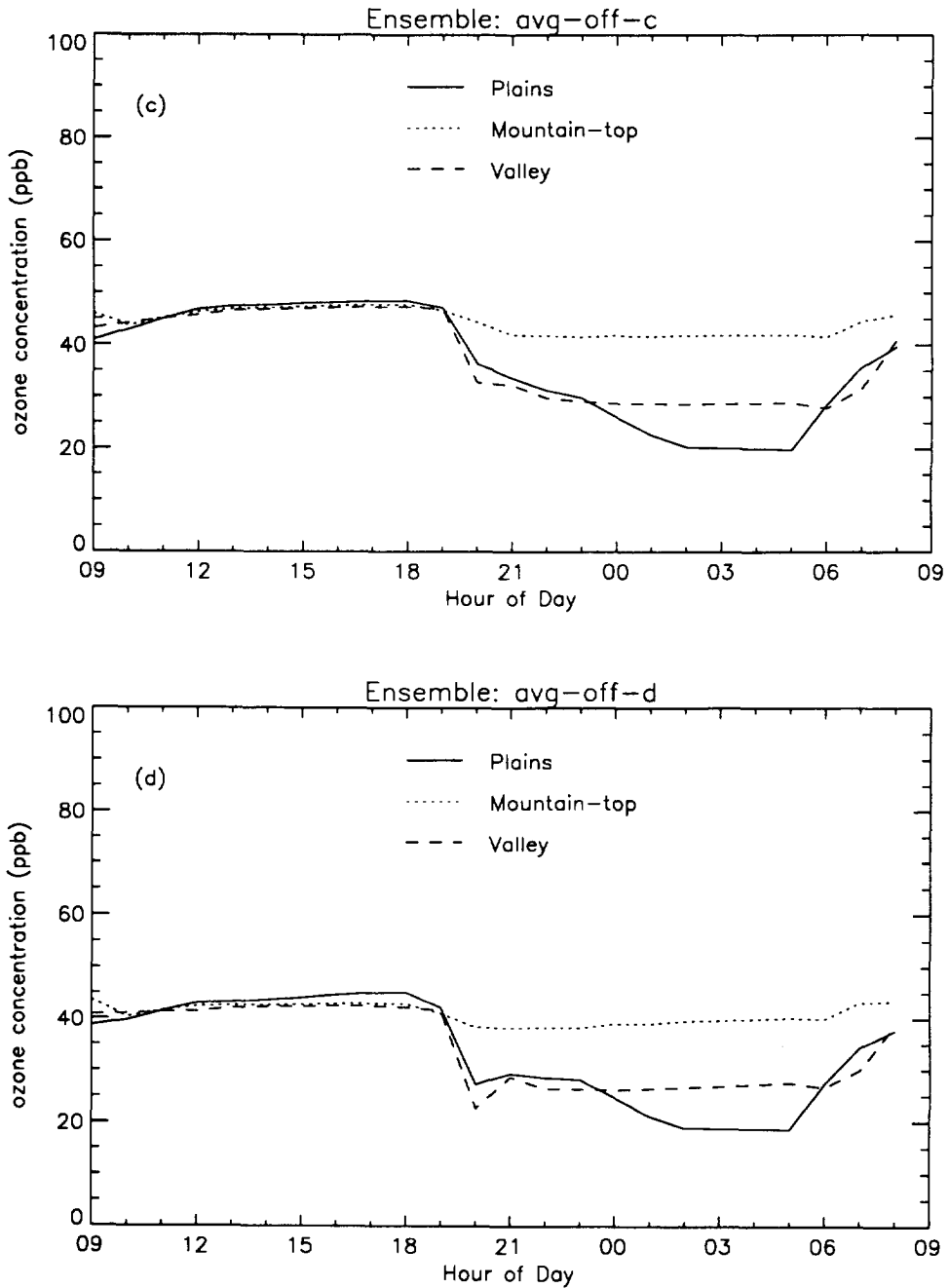


Fig. 8. Diurnal ensemble averages of ozone concentrations (ppb): (a) avg-on-c; (b) avg-on-d; (c) avg-off-c; and (d) avg-off-d (over western locations).

flow continues to transport a relatively constant mixing ratio of ozone to the mountaintop and its slopes (see also Fig. 5b).

4.3. Ozone flux and dosage at different elevations

Amounts of ozone deposited at the ground at various elevations and ozone dosage near the surface during daytime (0600 to 2000 CDT) and nighttime (2100 to 0500 CDT) are given in Table 3 for simulated ensemble (avg-on-d). The model results suggest that

less variation in daytime values of ozone flux and dosage occur at different elevations as compared to nighttime values. Even though nighttime ozone fluxes are only 10–20% of daytime values, nighttime ozone dosages at mountaintop and slope locations are greater than 50% of daytime values, while the nighttime dosage at the plains location is only 30% of its daytime value. Thus, our model results indicate that mountaintops and slopes experience higher ozone dosages throughout a diurnal cycle than do

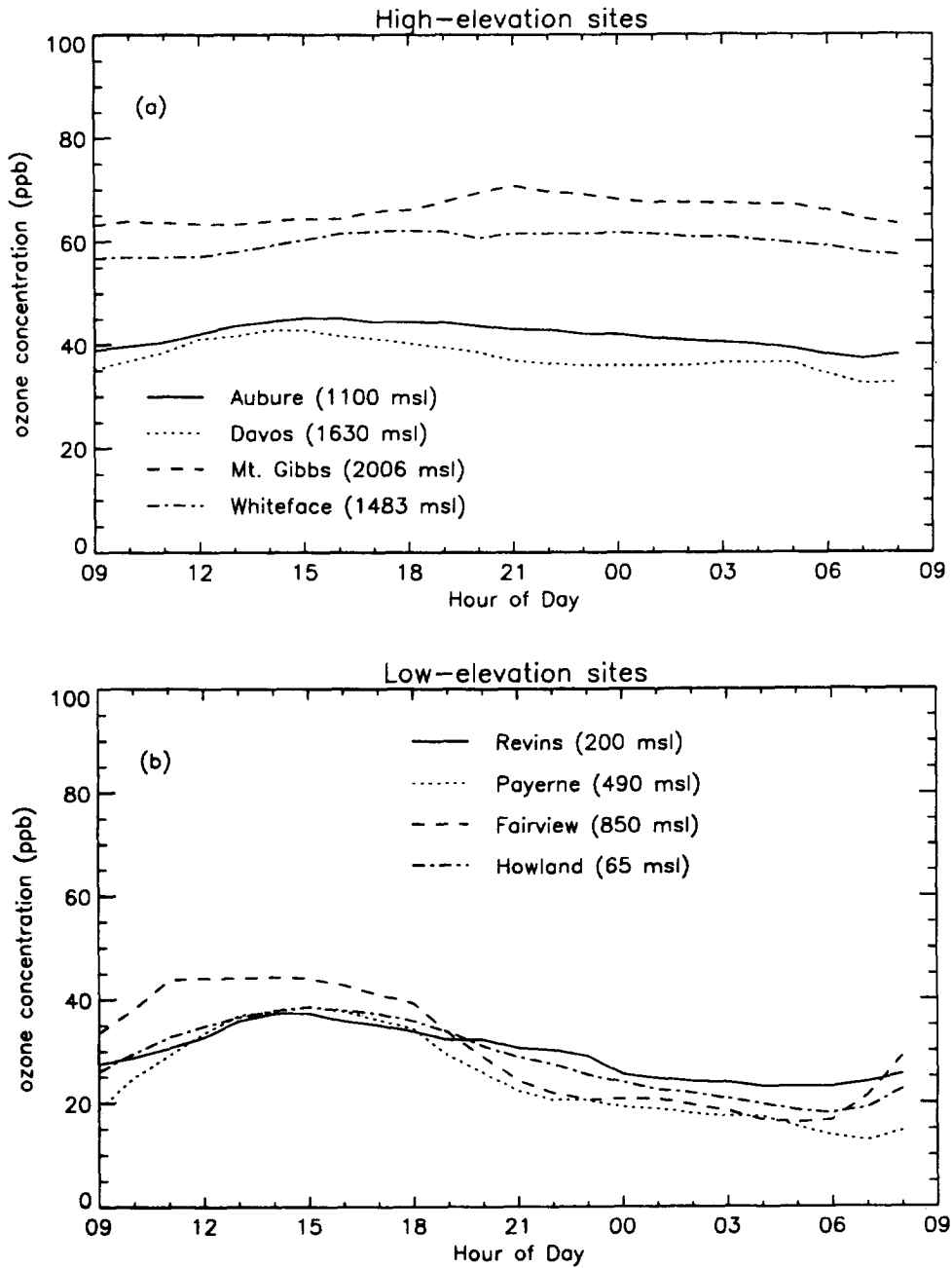


Fig. 9. Typical diurnal ozone concentration patterns (ppb) observed at selected low and high-elevation sites. Sources: Davos and Payerne, Wunderli and Gehrig (1990); Mt. Gibbs and Fairview, Aneja *et al.* (1991); Aubure and Revins, Proyou *et al.* (1991); Whiteface and Howland, Aneja and Li (1992).

Table 3. Ozone flux (10^{16} molecules cm^{-2}) and dosage (ppb hour) at the surface over western mountain ridge for simulated ensemble (avg-on-d)

Location	Elevation m.s.l.	Daytime flux	Nighttime flux	Daytime dosage	Nighttime dosage
Plains	0	5.018	0.563	696.8	216.5
Western slope	513	5.065	0.963	743.0	390.2
Mountaintop	950	4.969	0.937	761.0	395.6
Eastern slope	513	5.085	0.984	752.6	398.4
Valley	289	5.055	0.726	717.0	285.6

nearby lower-elevation locations. This may be a contributing factor in the observed decline of high-elevation forests in North America and central Europe and deserves further study.

5. CONCLUSIONS

In this investigation, the STEM-II chemistry/transport/deposition model, coupled with meteorological data from a two-dimensional hydrostatic mesoscale meteorological model, has been used to analyze ozone formation and transport in rural mountainous regions representative of the southeastern United States. The study has investigated the roles of the various processes of chemistry, dry deposition, and turbulent transport involved in this complex coupled atmospheric phenomenon. In general, mountainous regions experience higher ozone exposure throughout the diurnal cycle than do similarly located lower-elevation sites. Our model simulations suggest that this behavior is primarily due to the occurrence of local topographically induced wind systems coupled with photochemical processes. Higher nighttime surface ozone mixing ratios near the mountaintops were caused largely by the occurrence of nocturnal katabatic winds over the mountainslopes which advect ozone-rich air from aloft and maintain a high level of turbulent connectivity to air at higher levels. Larger ozone concentrations may also be observed as a result of the transport of an ozone-rich air mass above the NBL to the mountaintop as indicated by the case with low mean wind speed of 1 m s^{-1} (Fig. 5a).

The valley bottom experiences relatively higher ozone deposition than the plains regions due to the katabatic winds which continuously supply ozone-rich air to the valley slopes. The cross-valley wind system is quite efficient in destroying ozone by surface removal. Depletion of ozone in the valley, where the air is confined, occurs throughout the nocturnal boundary layer due to these cross-valley recirculations. However, over plains regions, ozone destruction is limited to a very shallow surface layer.

As with all numerical simulation studies, there are uncertainties. To better resolve whether rural, high-elevation, mountainous regions are NO_x limited or not, both anthropogenic and biogenic emissions should be included in future numerical studies. Biogenic hydrocarbon chemistry should be included in future simulations to study the effects of natural emissions in high-elevation forest regions.

Also, it is noted that because an idealized terrain together with a two-dimensional hydrostatic simulation is used in this study, the resolved slope flows, and their diurnal variations, may not quantitatively resemble those over realistic three-dimensional complex terrains. Modeled vertical motions over a mountainous terrain may differ by up to an order-of-magnitude at the same location for each

order-of-magnitude difference in grid size. Thus, the relative contribution of turbulence versus advection as modeled in these simulations may be different for different grid spacing. This problem, which concerns the complicated diurnal evolution of the balancing between the advective and turbulence effects in the presence of realistic three-dimensional complex terrain, will be discussed quantitatively in a future paper with an emphasis on physical effects.

Acknowledgements—This research is part of the Southern Oxidant Study (SOS)—a collaborative university, government, and private industry study to improve scientific understanding of the accumulation and effects of photochemical oxidants. Financial and in-kind support for SOS research and assessment activities is provided by the Environmental Protection Agency, National Oceanic and Atmospheric Administration, Department of Energy, Tennessee Valley Authority, Electric Power Research Institute, The Southern Company, Coordinating Research Council, Duke Power Company, and the States of Alabama, Florida, Georgia, Kentucky, Louisiana, Mississippi, North Carolina, South Carolina, Tennessee, and Texas. Acknowledgements are also made to the Center for Computational Sciences at the University of Kentucky, the Atmospheric Processes Group of the Earth and Environmental Sciences Center at Battelle Pacific Northwest Laboratory, and the Laboratory for Scientific Visual Analysis at Virginia Tech, for the computer resources used in the work. Much of this research was conducted while two of the authors were at the University of Kentucky. Pacific Northwest Laboratory is operated for the U.S. Department of Energy by Battelle Memorial Institute under contract DE-AC06-76RLO 1830.

REFERENCES

- Aneja V. P. and Li Z. (1992) Characterization of ozone at high elevation in the eastern United States: trends, seasonal variations, and exposure. *J. geophys. Res.* **97**, 9873–9888.
- Aneja V. P., Businger S., Li Z., Claiborn C. S. and Murthy A. (1991) Ozone climatology at high elevation in southern Appalachians. *J. geophys. Res.* **96**, 1007–1021.
- Angle R. P. and Sandhu H. S. (1989) Urban and rural ozone concentrations in Alberta, Canada. *Atmospheric Environment* **23**, 215–221.
- Atkinson R., Lloyd A. C. and Wines L. (1982) An updated chemical mechanism for hydrocarbon/ NO_x / SO_2 photo-oxidants suitable for inclusion in atmospheric simulation models. *Atmospheric Environment* **16**, 1341–1355.
- Broder B., Dütsch H. U. and Graber W. (1981) Ozone fluxes in the nocturnal planetary boundary layer over hilly terrain. *Atmospheric Environment* **15**, 1195–1199.
- Broder B. and Gygas H. A. (1985) The influence of locally induced wind systems on the effectiveness of nocturnal dry deposition of ozone. *Atmospheric Environment* **19**, 1627–1637.
- Businger J. A., Wyngaard J. C., Izumi Y. and Bradley E. F. (1971) Flux profile relationships in the atmospheric surface layer. *J. Atmos. Sci.* **28**, 181–189.
- Carmichael G. R., Peters L. K. and Saylor R. D. (1991) The STEM-II regional-scale acid deposition and photochemical oxidant model—I. An overview of model development and applications. *Atmospheric Environment* **25A**, 2077–2090.
- Chang Y. S., Carmichael G. R., Kurita H. and Ueda H. (1989) The transport and formation of photochemical oxidants in central Japan. *Atmospheric Environment* **23**, 363–393.

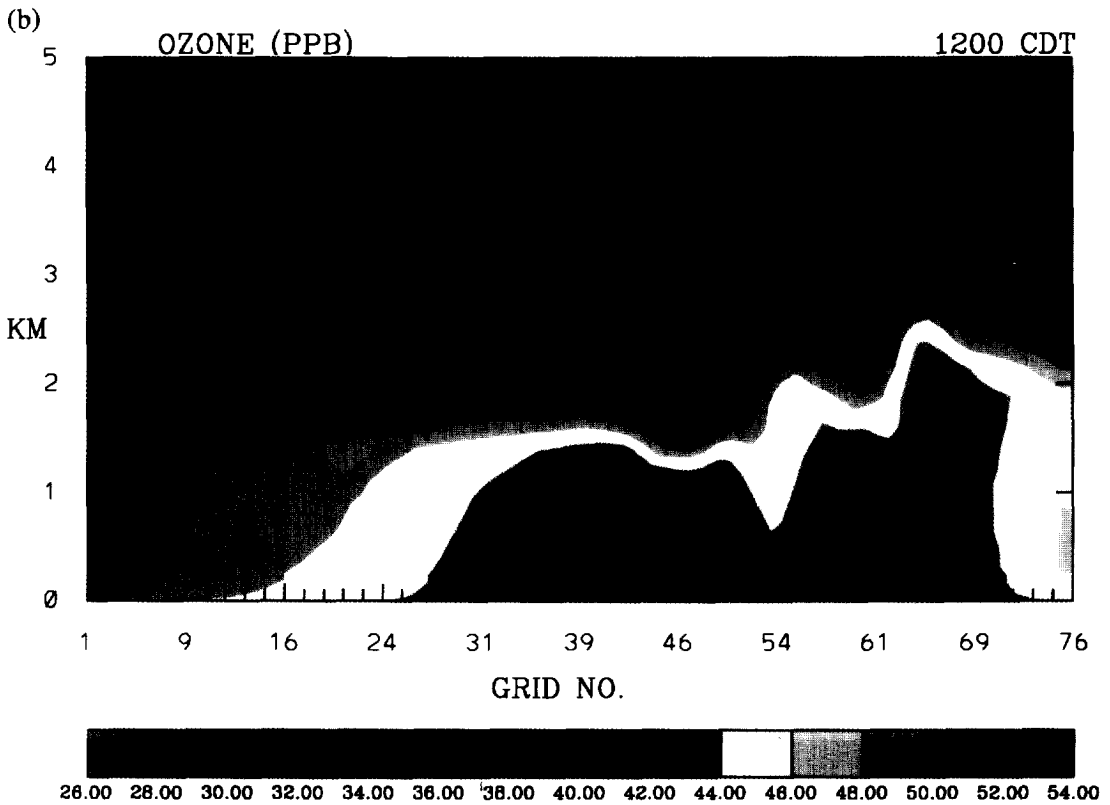
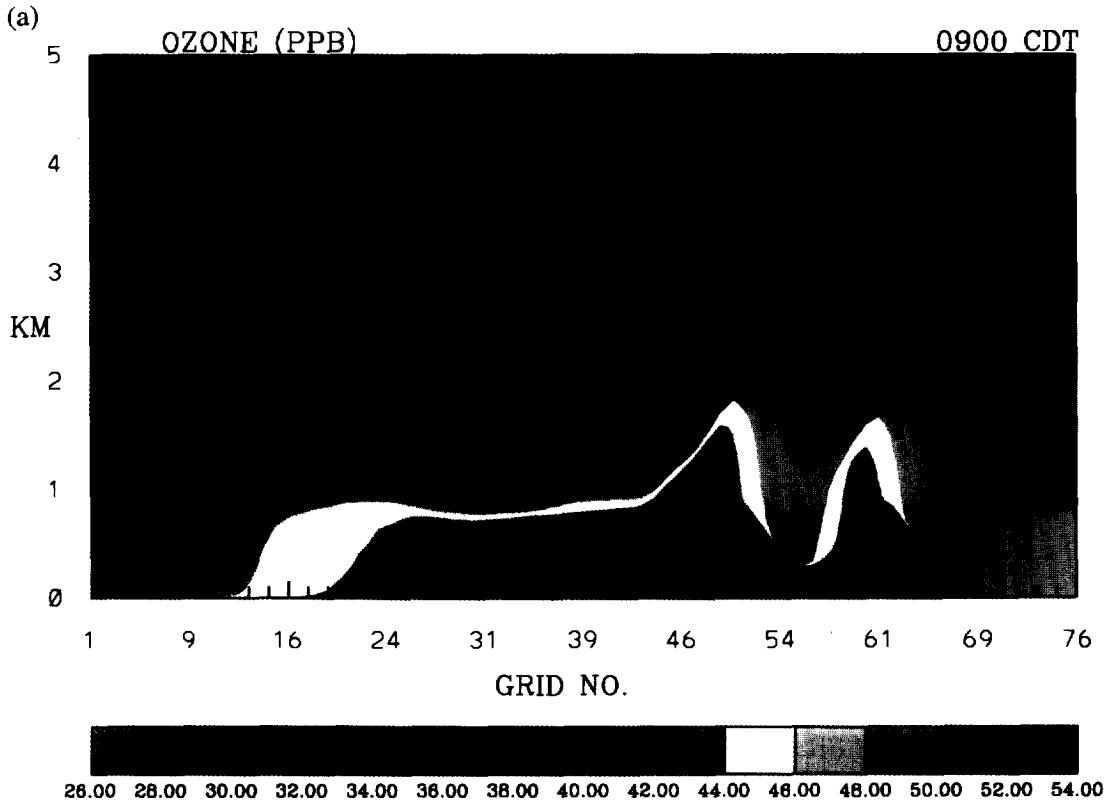


Fig. 10. (a, b).

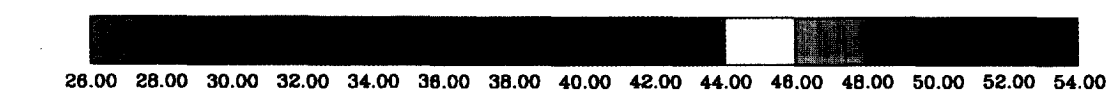
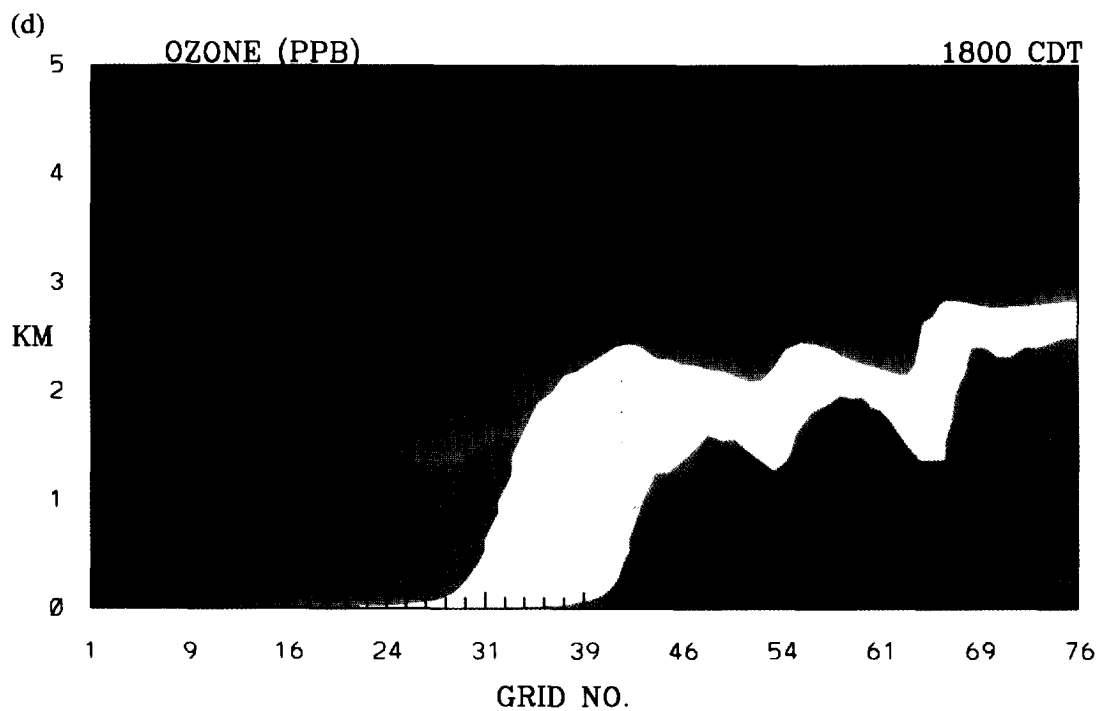
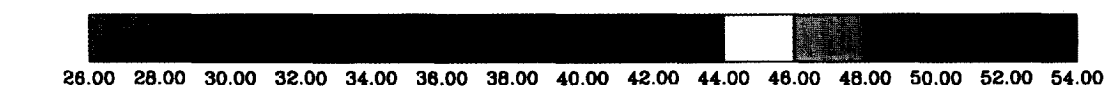
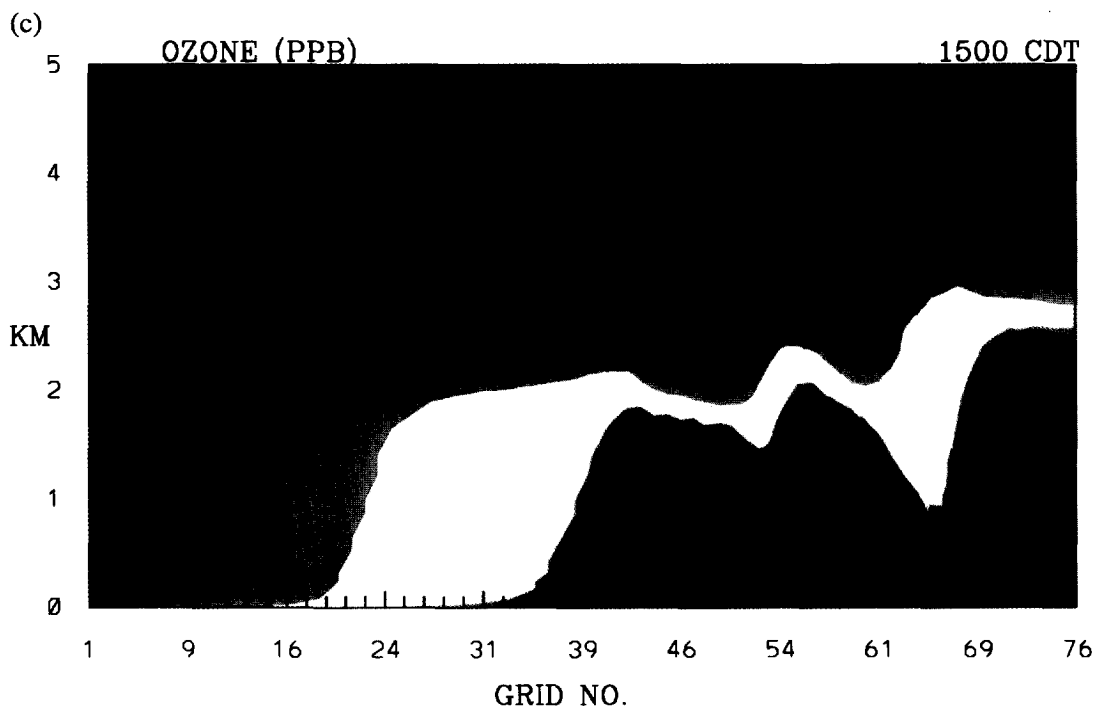


Fig. 10. (c, d).

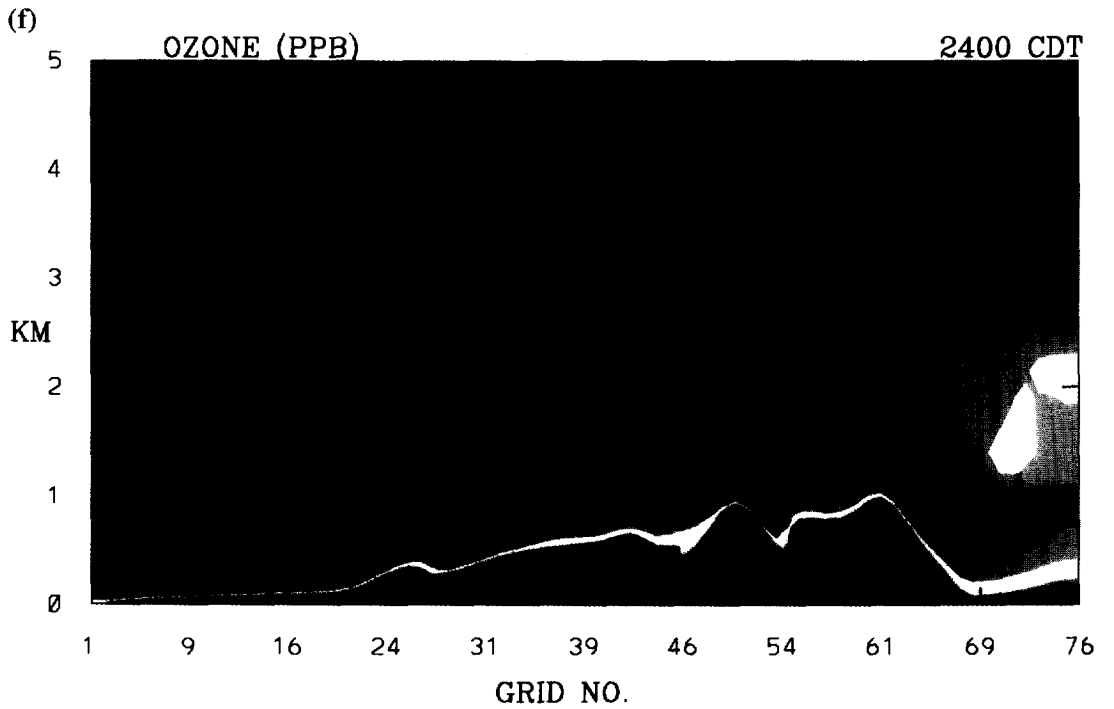
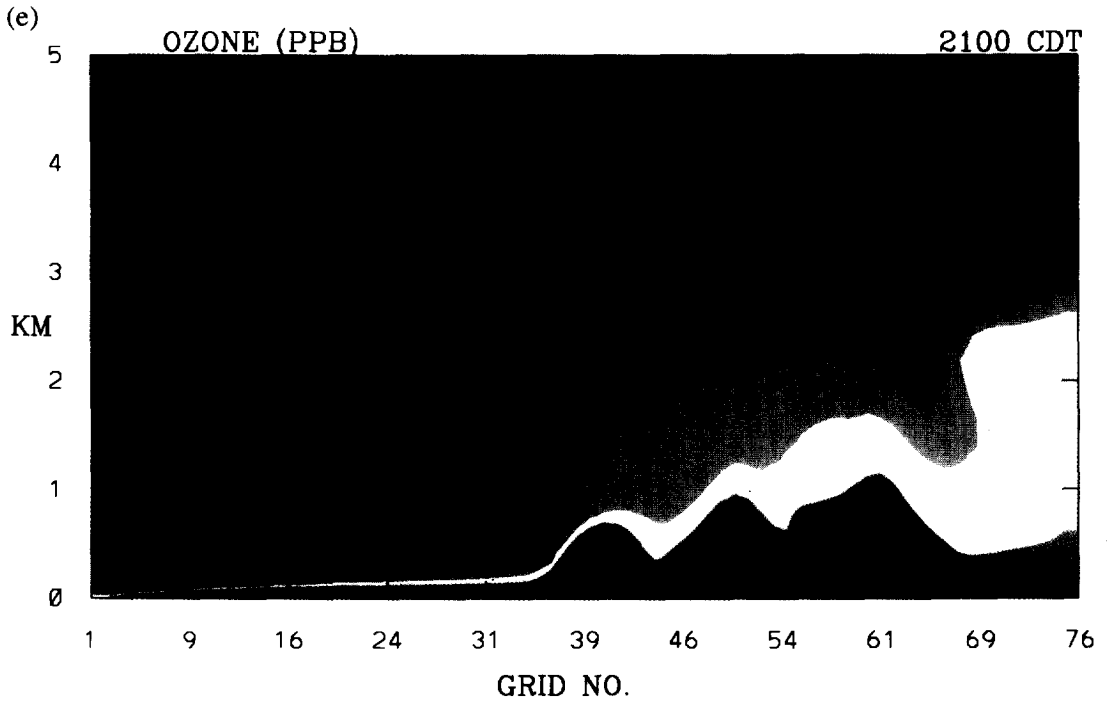


Fig. 10. (e, f).

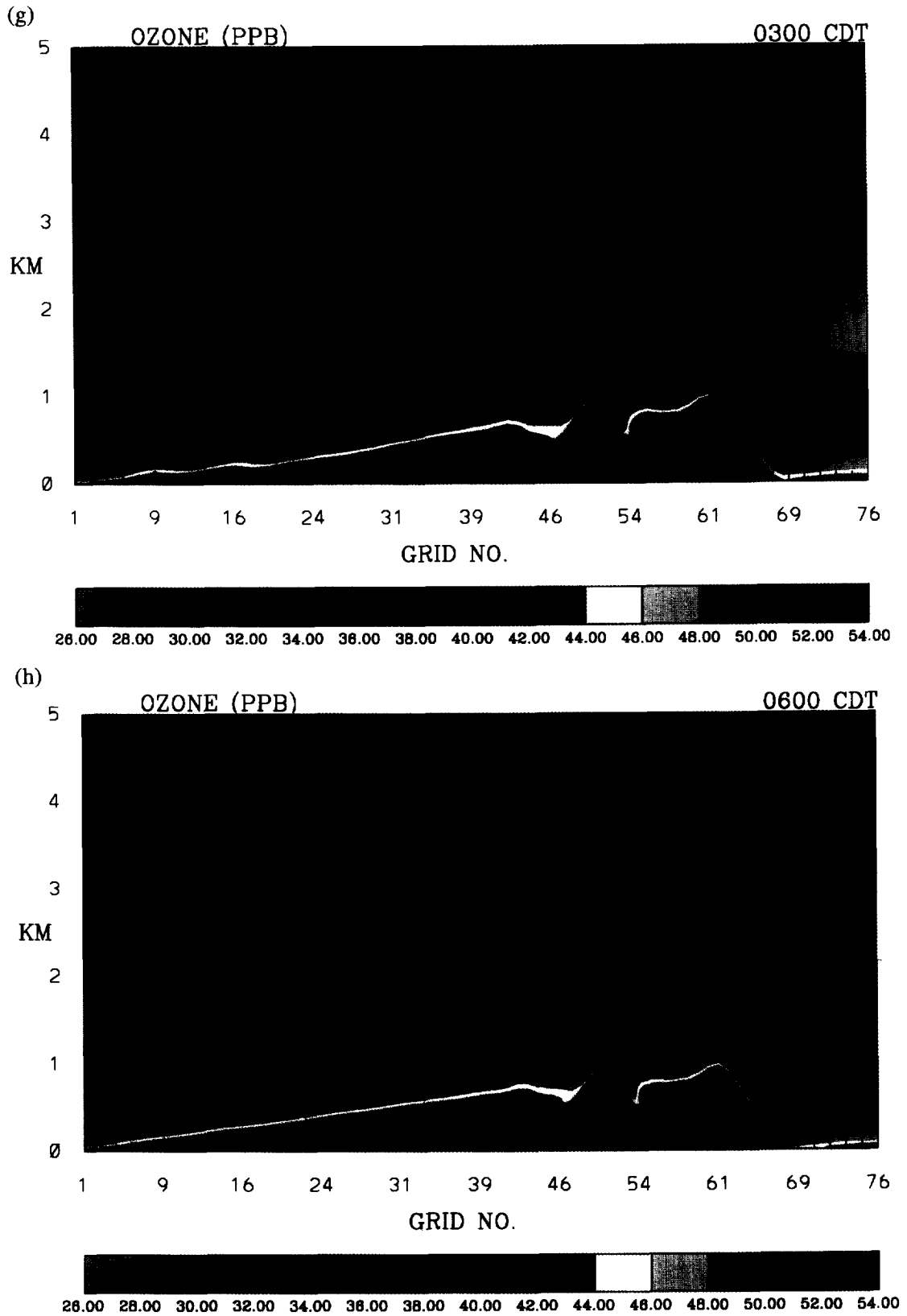


Fig. 10. Vertical ozone concentration contour plots (ppb) for simulation b-3-off-d at (a) 0900 CDT, (b) 1200 CDT, (c) 1500 CDT, (d) 1800 CDT, (e) 2100 CDT, (f) 2400 CDT, (g) 0300 CDT, and (h) 0600 CDT.

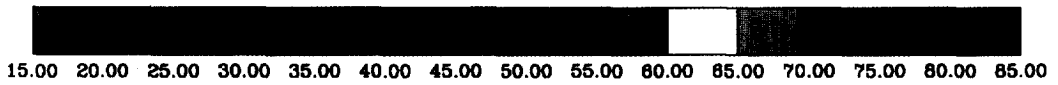
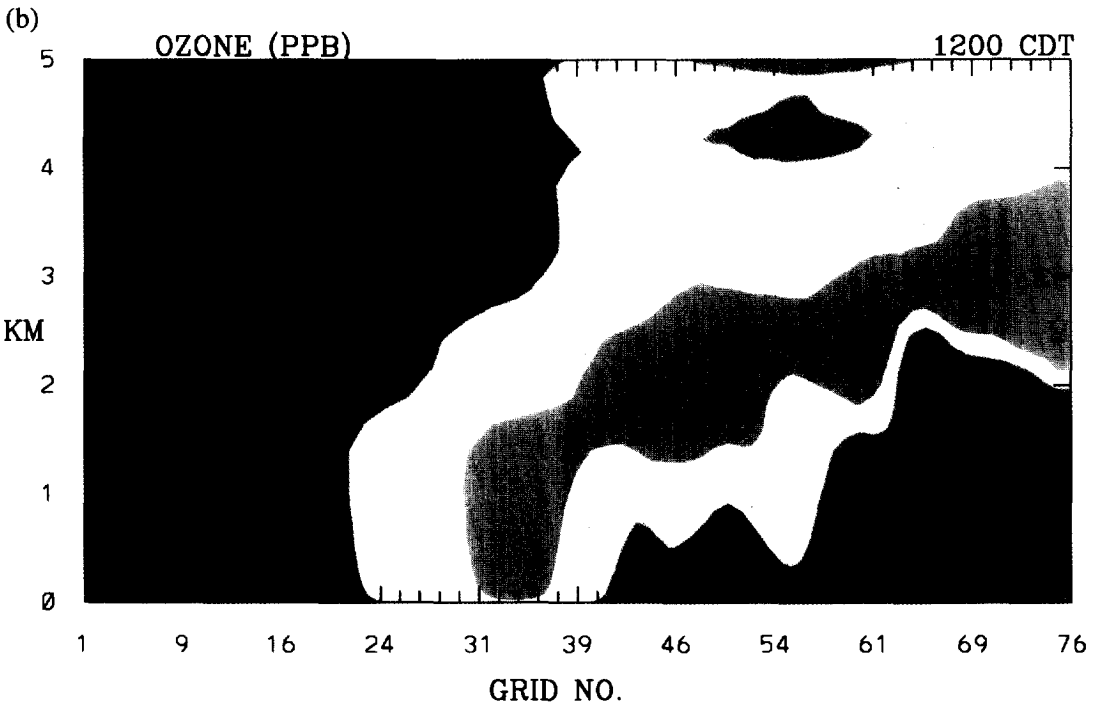
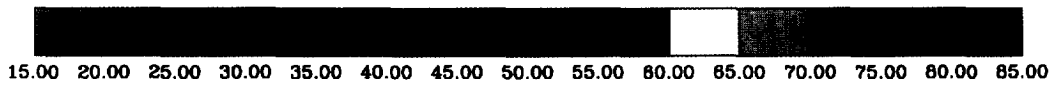
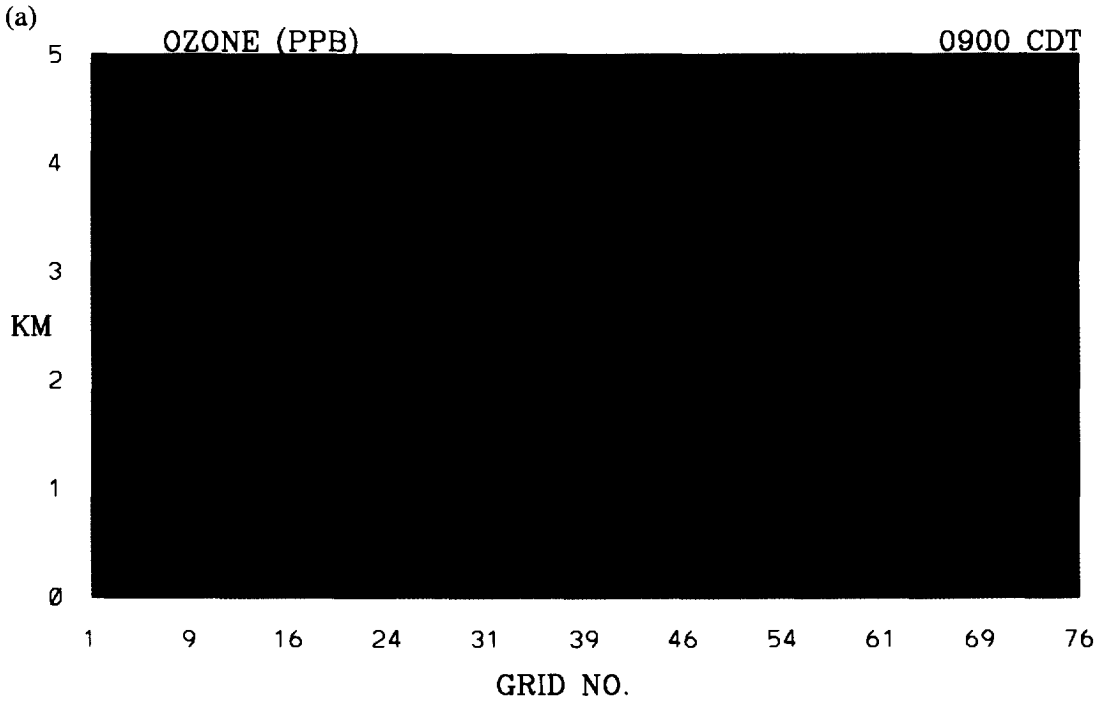


Fig. 11. (a, b).

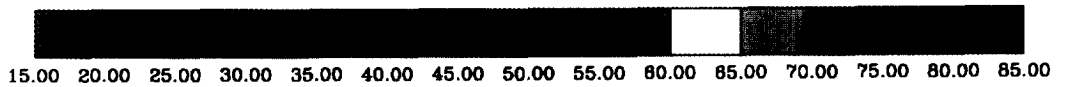
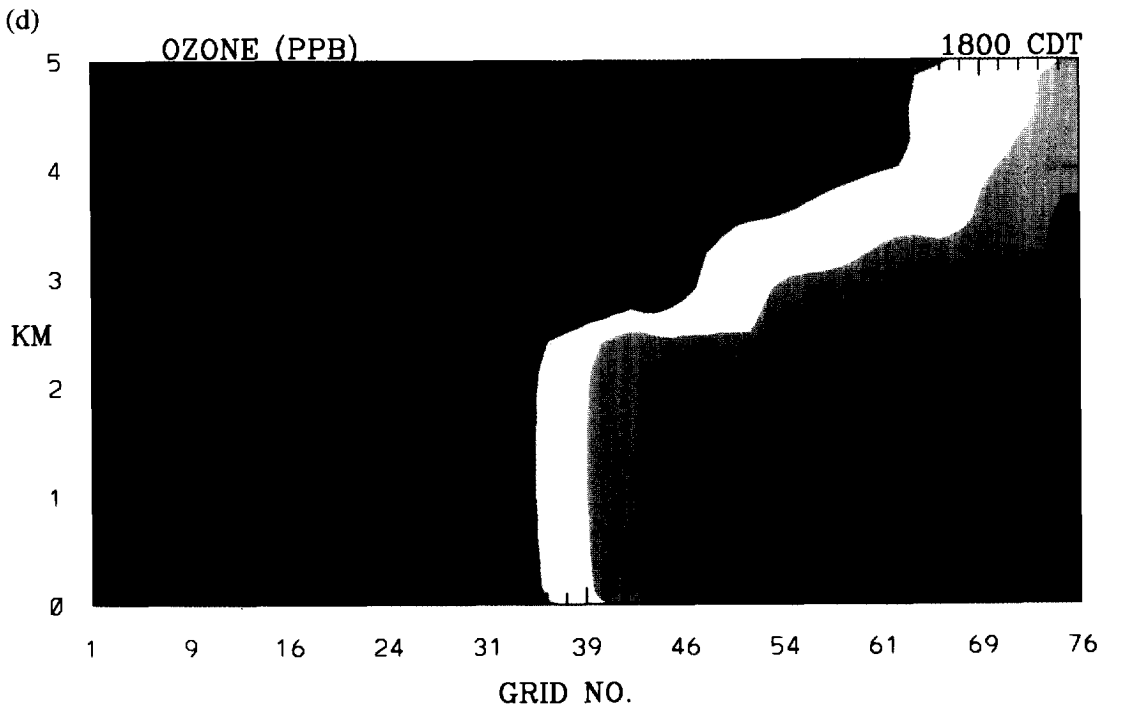
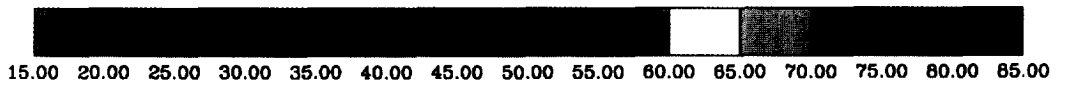
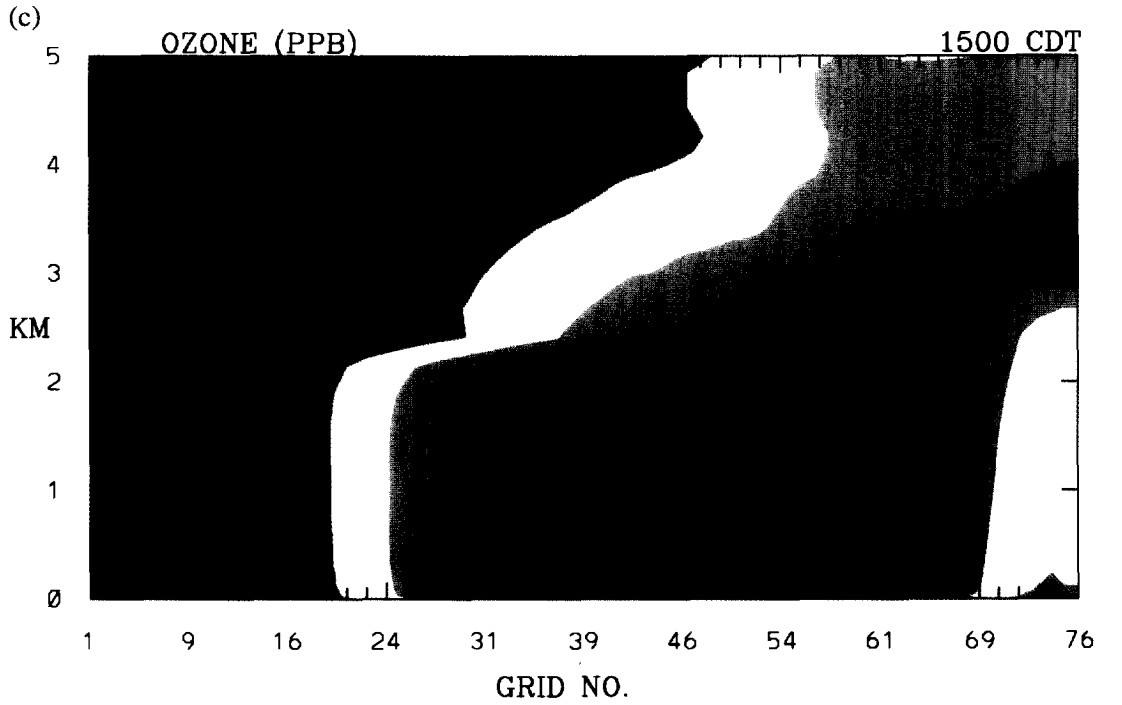


Fig. 11. (c, d).

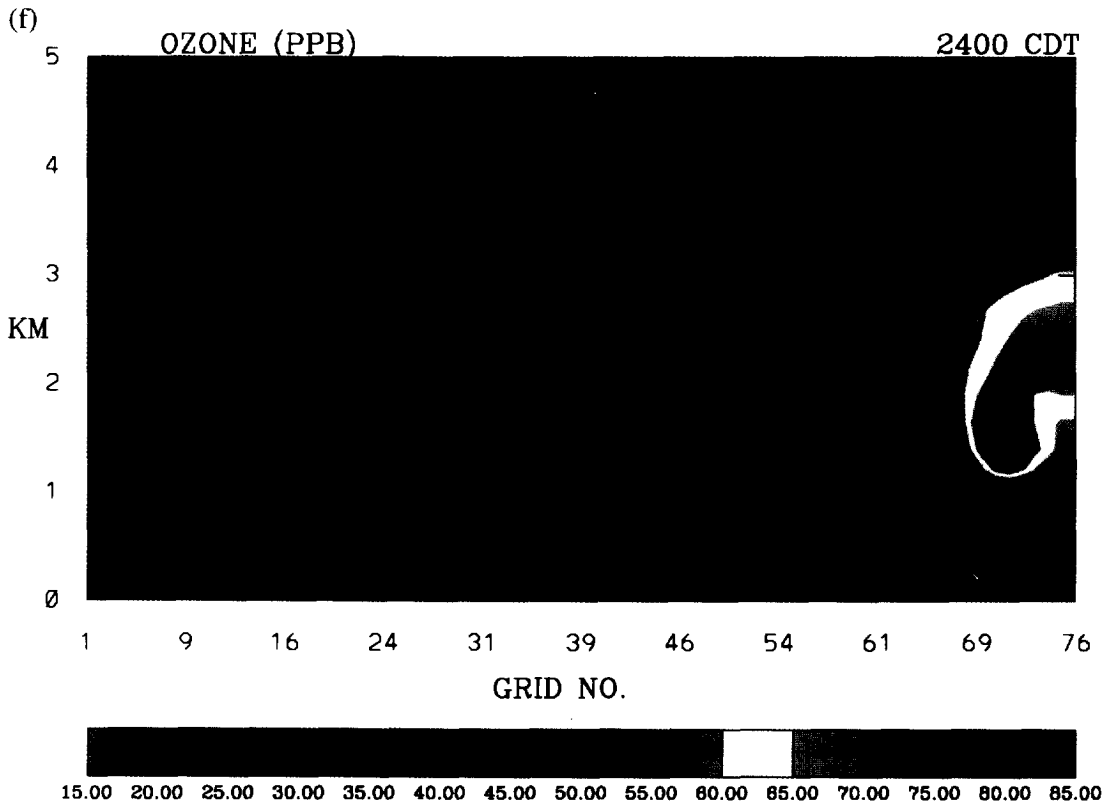
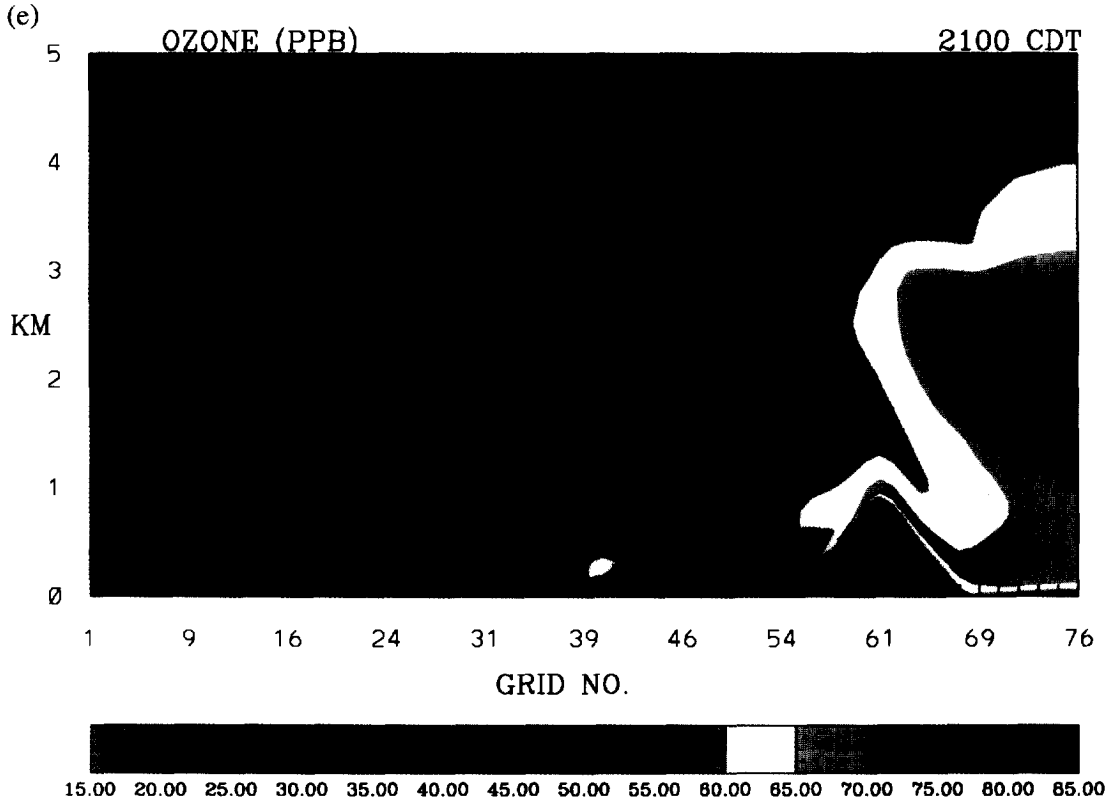


Fig. 11. (e,f).

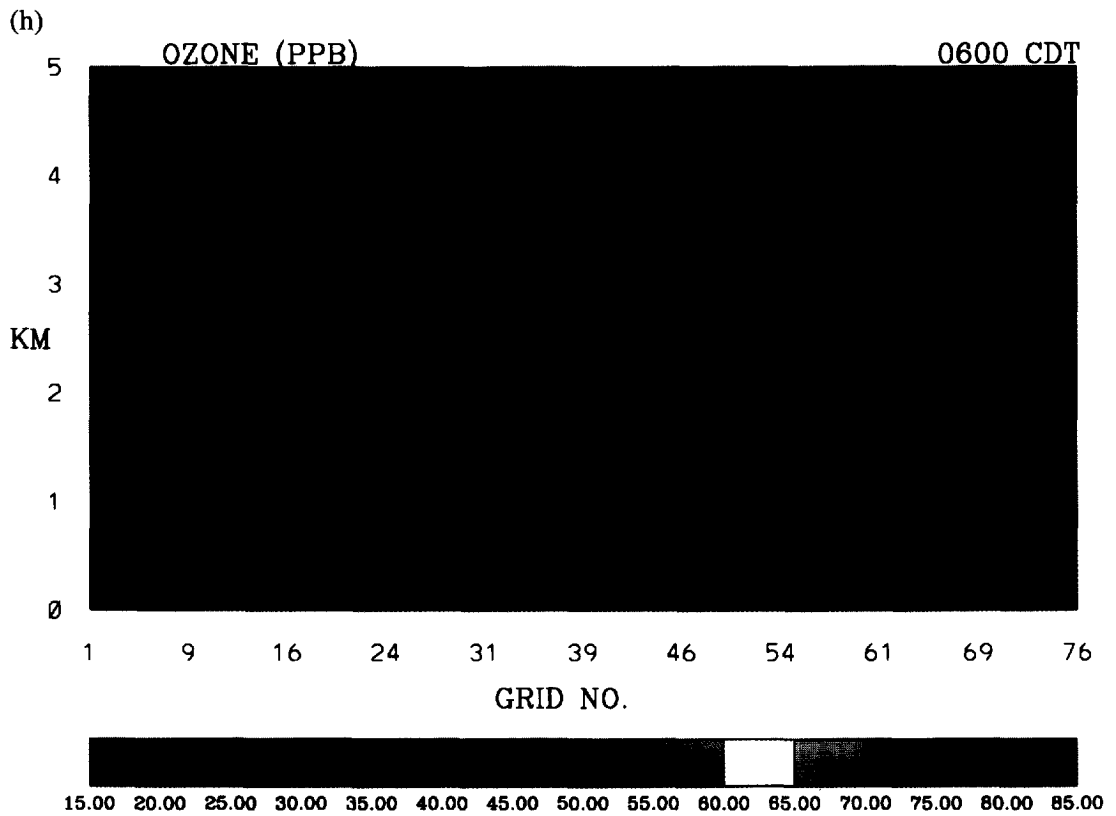
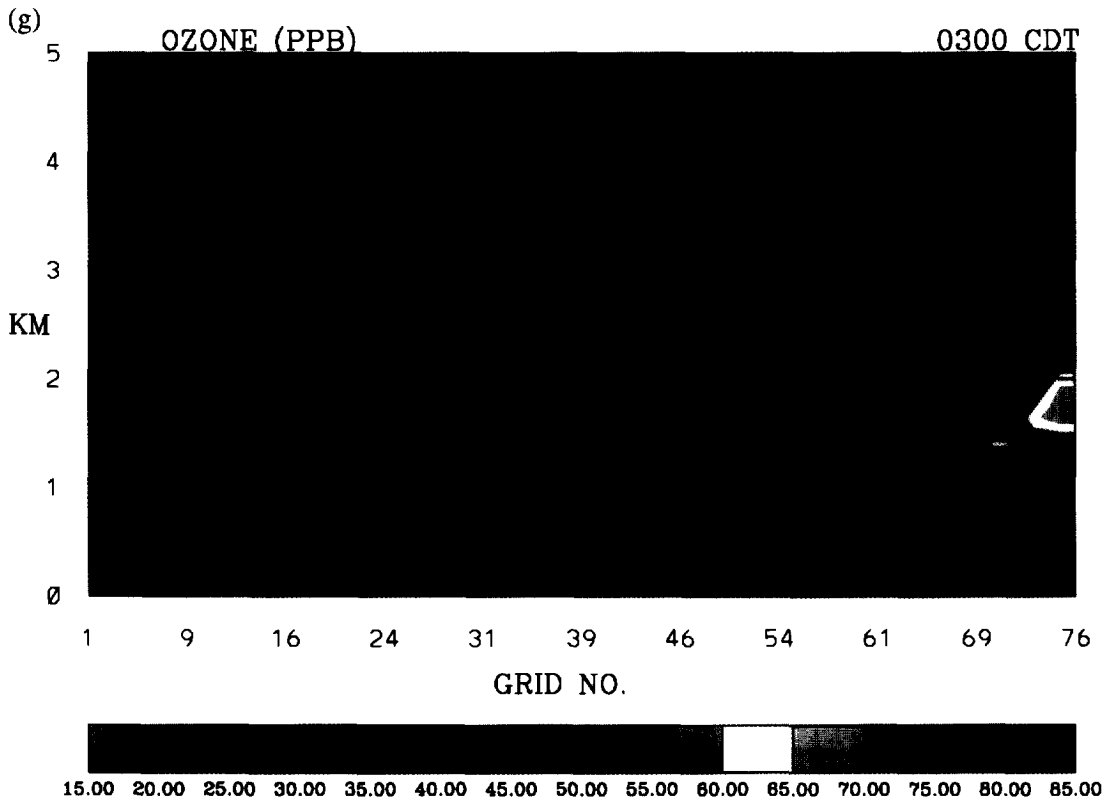


Fig. 11. Vertical ozone concentration contour plots (ppb) for simulation b-3-on-d at (a) 0900 CDT, (b) 1200 CDT, (c) 1500 CDT, (d) 1800 CDT, (e) 2100 CDT, (f) 2400 CDT, (g) 0300 CDT, and (h) 0600 CDT.

- Deardorff J. W. (1974) Three-dimensional numerical study of the height and mean structure of a heated planetary boundary layer. *Boundary-Layer Met.* **7**, 81–106.
- Fehsenfeld F. C., Bollinger M. J., Liu S. C., Parrish D. D., McFarland M., Trainer M., Kley D., Murphy P. C. and Albritton D. L. (1983) A study of ozone in the Colorado mountains. *J. Atmos. Chem.* **1**, 87–105.
- Fontan J., Minga A., Lopez A. and Druilhet A. (1992) Vertical ozone profiles in a pine forest. *Atmospheric Environment* **26A**, 863–869.
- Galbally I. E., Miller A. J., Hoy R. D., Ahmet S., Joynt R. C. and Attwood D. (1986) Surface ozone at rural sites in the Latrobe Valley and Cape Grim, Australia. *Atmospheric Environment* **20**, 2403–2422.
- Harrison M., Holman C. D., McCartney H. A. and McIlveen J. F. R. (1978) Short communication: nocturnal depletion of photochemical ozone at a rural site. *Atmospheric Environment* **12**, 2021–2026.
- Hanson P. J. and Lindberg S. E. (1991) Dry deposition of reactive nitrogen compounds: a review of leaf, canopy and non-foliar measurements. *Atmospheric Environment* **25A**, 1615–1634.
- Helas G., Broll A., Rumpel K.-J. and Warneck P. (1987) On the origins of night-time NO at a rural measurement site. *Atmospheric Environment* **21**, 2285–2295.
- Kelly N. A., Wolff G. T. and Ferman M. A. (1984) Sources and sinks of ozone in rural areas. *Atmospheric Environment* **18**, 1251–1266.
- Lefohn A. S. and Runeckels V. C. (1987) Establishing standards to protect vegetation—ozone exposure/dose considerations. *Atmospheric Environment* **21**, 561–568.
- Lovett G. M. and Kinsman J. D. (1990) Atmospheric pollutant deposition to high-elevation ecosystems. *Atmospheric Environment* **24A**, 2767–2786.
- Mahrer Y. and Pielke R. A. (1977) A numerical study of the air flow over irregular terrain. *Contr. Atmos. Phys.* **50**, 98–113.
- Mahrer Y. and Pielke R. A. (1978) A test of an upstream spline interpolation technique for the advective terms in a numerical mesoscale model. *Mon. Wea. Rev.* **104**, 1392–1402.
- McNider R. T. and Pielke R. A. (1981) Diurnal boundary-layer development over sloping terrain. *J. Atmos. Sci.* **38**, 2198–2212.
- McNider R. T. and Pielke R. A. (1984) Numerical simulation of slope and mountain flows. *J. Clim. appl. Met.* **23**, 1441–1453.
- O'Brien J. J. (1970) A note on the vertical structure of the eddy exchange coefficient in the planetary boundary layer. *J. Atmos. Sci.* **27**, 1213–1215.
- Padro J., den Hartog G. and Neumann H. H. (1991) An investigation of the ADOM dry deposition module using summertime O₃ measurements above a deciduous forest. *Atmospheric Environment* **25A**, 1689–1704.
- Peake E. and Fong B. D. (1990) Ozone concentrations at a remote mountain site and at two regional locations in southwestern Alberta. *Atmospheric Environment* **24A**, 475–480.
- Pielke R. A. (1974) A three-dimensional numerical model of the sea breeze over South Florida. *Mon. Wea. Rev.* **102**, 115–139.
- Pielke R. A. and Mahrer Y. (1975) Techniques to represent the heated planetary boundary layer in mesoscale models with coarse vertical resolution. *J. Atmos. Sci.* **32**, 2288–2308.
- Proyou A. G., Toupance G. and Perros P. E. (1991) A two-year study of ozone behaviour at rural and forested sites in eastern France. *Atmospheric Environment* **25A**, 2145–2153.
- Reich P. B. and Amundson A. G. (1985) Ambient levels of ozone reduce net photosynthesis in tree and crop species. *Science* **230**, 566–570.
- Saylor R. D., Peters L. K. and Mathur R. (1991) The STEM-II regional-scale acid deposition and photochemical oxidant model—III. A study of mesoscale acid deposition in the lower Ohio River Valley. *Atmospheric Environment* **25A**, 2873–2894.
- Seinfeld J. H. (1989) Urban air pollution: state of the science. *Science* **243**, 745–752.
- Stull R. B. (1988) *An Introduction to Boundary Layer Meteorology*. Kluwer, Boston.
- Warneck P. (1988) *Chemistry of the Natural Atmosphere*, pp. 176–222. Academic Press, San Diego, California.
- Woodman J. N. and Cowling E. B. (1987) Airborne chemical and forest health. *Envir. Sci. Technol.* **21**, 120–126.
- Wunderli S. and Gehrig R. (1990) Surface ozone in rural, urban and alpine regions of Switzerland. *Atmospheric Environment* **24A**, 2641–2646.
- Zaveri R. A. (1993) A diagnostic modeling study of summertime diurnal ozone behavior in rural mountainous locations, M.S. thesis, Department of Chemical Engineering, University of Kentucky, Lexington, Kentucky.